Distribution of carbon isotopes in the glacial ocean: A model study

Michel Crucifix[1]

Institut d'Astronomie et de Géophysique G. Lemaître, Louvain-la-Neuve, Belgium

Received 7 January 2005; revised 5 July 2005; accepted 13 September 2005; published 14 December 2005.

[1] A series of simulations are conducted with a global climate model of intermediate complexity (MoBidiC). This model includes ocean circulation dynamics, including the carbon cycle, coupled to a zonally averaged atmosphere. Oceanic distributions of nutrients, apparent oxygen utilization, radiocarbon, and carbon 13 are discussed for the preindustrial era (validation) as well as three states of the glacial ocean, termed interstadial (very active formation of deep water in the North Atlantic Ocean), stadial (moderate convection and important flow of Antarctic Deep Water in the Atlantic), and Heinrich (no formation of North Atlantic Deep Water). The stadial and interstadial states are stable. The Heinrich state is forced by a continuous freshwater discharge into the North Atlantic. The model exhibits significant changes in the isotopic composition of the ocean between the three modeled glacial states. Results for $\delta^{13}C$ tend to be in qualitative agreement with paleoceanographic data, except that the model fails at representing the strong depletion in $\delta^{13}C$ in the Southern Ocean. The Heinrich Atlantic Ocean is older than the stadial ocean at all depths (up to 1500 years). The "interstadial" ocean has younger deep water and older intermediate water than the "stadial." It is recognized that the simulated changes in intermediate water age are less reliable because of the structure of the model. Color tracers are used to show that changes in the isotopic composition of Atlantic bottom water are mainly related to a redistribution of water masses. A simple method is tested, by which it is possible to reconstruct the North Atlantic water flow from the zonal profiles of salinity and $\Delta^{14}C$. Finally, dividing artificially the gas exchange rate in the Southern Ocean by four results in a 0.4‰ decrease in the $\delta^{13}C$ of Antarctic Bottom Water. Changes in new production are, comparatively, less effective at altering the $\delta^{13}C$ ratio.

Citation: Crucifix, M. (2005), Distribution of carbon isotopes in the glacial ocean: A model study, *Paleoceanography*, *20*, PA4020, doi:10.1029/2005PA001131.

1. Introduction

[2] The ratio between the masses of ^{13}C and ^{12}C preserved in the carbonate shells of foraminifera can be used to reconstruct the history of ocean circulation over timescales of thousands years [e.g., *Duplessy et al.*, 1988; *Vidal et al.*, 1997; *Curry and Oppo*, 2005]. Furthermore, the difference between surface and deep water age may be estimated by comparing the radiocarbon concentrations of planktonic (living in the mixed layer) and benthic (living at depth) foraminifera [*Duplessy et al.*, 1989]. Where independent chronostratigraphic constraints exist (e.g., oxygen isotope stratigraphy [*Walbroeck et al.*, 2001]), it is possible to use the planktonic $\Delta^{14}C$ to infer the radiocarbon age of surface water (the reservoir age).

[3] These analyses, along with multiproxy reconstructions of sea surface temperature, salinity and other paleonutrient tracers such as Cd/Ca [*Boyle*, 1988], lead to the paradigm that the Atlantic Ocean circulation has undergone large-scale reorganizations during the last glacial period [*Maslin and Shackleton*, 1995; *Labeyrie et al.*, 1995]: (1) During the "interstadial" (warmer) phases identified in Greenland ice core records [*Dansgaard and Oeschger*, 1989; *Bond et al.*, 1993], the ocean was presumably well ventilated, with active convection in the Nordic Seas. (2) The Last Glacial Maximum (LGM) ocean was characterized by an intermediate (around 2000 m) water mass originating from the North Atlantic (the glacial North Atlantic Intermediate Water) sandwiched between intermediate and deep water of southern origin [*Duplessy et al.*, 1988; *Boyle*, 1995; *Curry and Oppo*, 2005]. (3) During Heinrich events [*Heinrich*, 1988; *Grousset et al.*, 1993], there was no deep convection in the North Atlantic. Deep water was exclusively of southern origin [*Sarnthein et al.*, 1994; *Maslin and Shackleton*, 1995; *Vidal et al.*, 1997].

[4] Reconstructing past ocean circulation from radiocarbon age and paleonutrients is not trivial. *Wunsch* [2003] cautions that local changes in $\Delta^{14}C$ have to be interpreted in terms of oceanic water masses; they are not necessarily related to a variation in the intensity of the North Atlantic overturning cell. On the other hand, $\delta^{13}C$ and $\Delta^{14}C$ are controlled by the carbon dioxide solubility in water, the piston velocity (controlling the gas exchange rate with the atmosphere), and sea ice cover. The fractionation ratio at the air-sea interface also slightly depends on the temperature [*Mook*, 1986]. *Broecker and Maier-Reimer* [1992] termed "thermodynamic effect" the dependence of surface water $\delta^{13}C$ on temperature related to the combination of these

[1]Now at Hadley Centre for Climate Prediction and Research, Met Office, Exeter, UK.

purely physical factors. Finally, surface $\delta^{13}C$ depends on the new production. As a consequence, changes in temperature, nutrients, or shortwave absorption in the euphotic zone may impact on the $\delta^{13}C$ content of ''end-members'' (NADW and AABW).

[5] Numerical modeling of the ocean circulation and isotopic tracers may help to address these issues. *Winguth et al.* [1999] explored the links between sea surface boundary conditions, deep-sea circulation and distribution of $\delta^{13}C$ and nutrients. They emphasized the sensitivity of both ocean circulation and nutrient distribution on surface salinity and zonal wind forcing in the Southern Ocean. *Stocker* [1998] and *Delaygue et al.* [2003] estimated with a zonally averaged ocean model that changes in ventilation rates may modify the radiocarbon concentration of surface water by as much as 35‰, and cause top-to-bottom radiocarbon age variations of the order of 1000 years. [*Meissner et al.*, 2003] performed a series of modern and glacial climate simulations with the UVic climate model and they found that the LGM climate simulation best compatible with data has an Atlantic meridional overturning cell about 40% less intense than today. This is in agreement with the *McManus et al.* [2004] estimate based on Pa/Th tracers. *Campin et al.* [1999] specifically addressed the role of sea ice cover: They showed that, with respect to today, increased Antarctic sea ice cover caused a reduction of radiocarbon content of deep Antarctic water while the water itself was, in their simulations, younger to today (with age defined by means of an ''age tracer'' assumed to be zero at the surface).

[6] The present study proposes to calculate the variations in $\Delta^{14}C$ and $\delta^{13}C$ between the stadial ocean and today, as well as those occurring between the stadial, interstadial and Heinrich states. The advance with respect to the above cited works is to explore the different states of the glacial ocean documented in the paleoceanography literature. It is also aimed at estimating the contributions of the changes in piston velocity, solubility and new production on the isotopic composition changes associated with the transitions between the stadial and interstadial phases. Finally, it is attempted to distinguish the changes in local composition of water caused by a modification of the properties of the main water masses (i.e., what is NADW made of?) from those caused by a change in water origin (i.e., how much of that water parcel comes from the North Atlantic?).

[7] To reach these goals, a series of sensitivity experiments have been performed with MoBidiC. MoBidiC is a model of intermediate complexity that includes the atmosphere, the ocean and its carbon cycle with a low resolution (5° in latitude, three basins in longitude). Our model has a much lower resolution than that used by *Campin et al.* [1999], *Winguth et al.* [1999], *Meissner et al.* [2003] and *Schmittner* [2003]. It is coupled to an atmospheric component (as given by *Meissner et al.* [2003], *Delaygue et al.* [2003] and *Schmittner* [2003]), so there is no need to prescribe salinity, temperature or surface fluxes.

[8] The model is described in section 2. Then I discuss the distributions of nutrients, $\delta^{13}C$ and $\Delta^{14}C$ in a control (preindustrial) experiment and compare them with available data. The corresponding distributions obtained for the three states of the glacial ocean (stadial, interstadial and Heinrich) are next presented and analyzed. Finally, sensitivity studies give insights into the impacts of changes in gas exchange rate, solubility and new production on these distributions.

2. Model Description

[9] MoBidiC's atmosphere is based on the zonally averaged, quasi-geostrophic equations, which are solved on two levels on the vertical with a horizontal resolution of 5° in latitude. The model also includes parameterizations for heat, moisture and momentum transports associated with the mean meridional circulation [*Gallée et al.*, 1991; *Crucifix et al.*, 2002]. Each zonal band is divided into up to 13 sectors of variable width for which the radiative transfer in the atmospheric column, as well as the snow, heat and moisture surface balances are calculated. A sector can be a continent (possibly snow covered), an ocean (possibly with sea ice), or an ice sheet.The oceans are represented by three basins (Atlantic, Pacific and Indian). For each of them, the zonally averaged primitive equations with rigid lid and Bousinesq approximations are explicitly solved on 19 unevenly spaced levels on the vertical (50- to 500-m resolution [*Hovine and Fichefet*, 1994]). Interbasin exchanges through the Arctic and Southern oceans are represented by interconnecting the basins in the north (Pacific and Atlantic) and in the south (Pacific, Atlantic and Indian), respectively. Bottom topography is accounted for according to the vertical resolution of the model. The model also includes parameterizations for downsloping currents and the Arctic surface gyre [*Crucifix et al.*, 2001]. Finally, the biogeochemical cycle includes 8 tracers: dissolved inorganic carbon (DIC), dissolved inorganic carbon 13 (DI13C), dissolved organic carbon (DOC), dissolved organic carbon 13 (DO13C), alkalinity (ALK), phosphates (PO4), oxygen (O2) and radiocarbon (14C). The processes governing the tracer sink/source terms are gas exchanges with the atmosphere, new production in the euphotic zone, remineralization of particulate carbon in the ocean, respiration of dissolved organic carbon, production and redissolution of biogenic carbonates in the ocean, and radioactive decay.

2.1. Surface Chemistry

[10] The pH is diagnosed by a Newton-Raphson iteration scheme resolving the constraints imposed by the carbonate, phosphates, silicates and boron acid-base systems. Silicates and boron concentrations are prescribed to modern observations (a rough assumption, but reasonable where the sole purpose is to calculate the pH). The equilibrium chemical constants of the different systems accounted for are functions of temperature and salinity after *Goyet and Poisson* [1989], *Dickson* [1990], and *Dickson and Riley* [1976].

2.2. Air-Sea Exchange

[11] The model explicitly calculates the air-sea fluxes of CO_2 and O_2 according to a piston velocity formulation:

$$F_{AirEx,DIC} = -k_{CO2}\left(CO_{2,aq} - pCO_2 sol_{CO2}\right) \quad (1)$$

$$F_{AirEx,O2} = -k_{O2}\left(O_{2,aq} - pO_2 sol_{O2}\right) \quad (2)$$

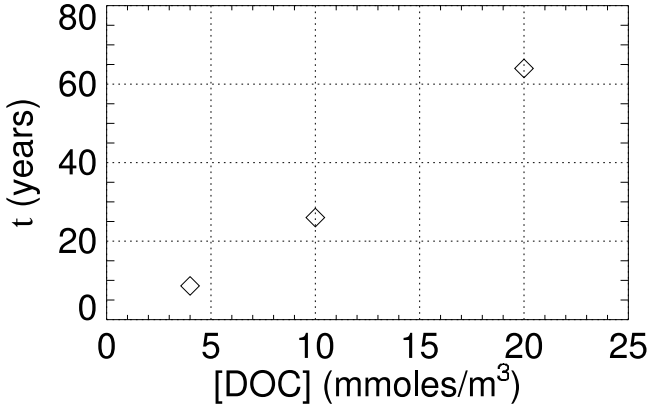

Figure 1. Characteristic time for DOC remineralization as a function of the mean DOC content of the global ocean, diagnosed to maintain the balance between DOC production and DOC remineralization. Experiments were done with a stand-alone version of the ocean component of MoBidiC, using prescribed distributions of sea surface temperature and salinity.

The generic notation $F_{X,Y}$ means the source of tracer Y due to the process X. CO_2,*aq* and O_2,*aq* stand for aqueous form concentrations in surface seawater; pCO_2 and pO_2 are the partial atmospheric pressures. Solubilities sol_{CO2} and sol_{O2} are function of surface temperature after *Weiss* [1970] and *Weiss* [1974], respectively. Piston velocities k_{CO2} and k_{O2} are given by *Wanninkhof* [1992]. They depend on wind velocity and include a chemical enhancement factor. The piston velocity is further scaled by the lead fraction (1 – fractional ice cover), and then multiplied by 3.31 to force the globally averaged surface piston velocity to be consistent with that obtained when using Wanninkhof's formulae with modern climatology. This factor allows us to correct for the underestimate of wind variability and meridional velocity. The changes in tracer surface concentration caused by precipitation and evaporation are represented by an additional source-sink term for each tracer (method of virtual fluxes).

2.3. New Production in the Euphotic Zone

[12] New production occurs in the euphotic zone, which is represented by the first two layers in the ocean (first 100 m). It is based on Michaelis-Menten kinetics assuming limitation by phosphates [*Maier-Reimer*, 1993]. The (negative) source of phosphates due to new production in the euphotic zone equals

$$F_{New,PO4} = -B\frac{PO4^2}{PO4 + \overline{PO4}} \tag{3}$$

$$B = 9.65 \cdot 10^{-8}\mathrm{s}^{-1}\mathrm{Q}\frac{\mathrm{T}+2}{\mathrm{T}+10}\frac{\mathrm{C}_0}{conv.depth} \tag{4}$$

where Q is the normalized incident shortwave radiation; T is the water temperature; C_0 = 50 m. The overbar indicates a global volume average. Source and sink terms for DIC, O2 and ALK associated with new production are calculated assuming constant Redfield factors given by *Anderson and Sarmiento* [1994]: DIC:PO4 = 117; O2:PO4 = −170; ALK:PO4 = −16. The produced organic carbon is partitioned in equal proportions between DOC and particulate organic carbon.

2.4. Respiration in the Aphotic Zone

[13] Respiration of dissolved organic carbon obeys a simple time decay rule:

$$F_{Resp,DIC} = -\frac{DOC}{\tau}. \tag{5}$$

Three sensitivity runs with the ocean stand-alone version of MoBidiC illustrate the interdependency between the characteristic respiration time τ and $\overline{DOC}$ at equilibrium (Figure 1). The standard version used for all experiments shown hereinafter uses a mean $\overline{DOC}$ of 4.2 μmol L^{-1}, corresponding to a turnaround time of 8.6 years. POC is instantaneously remineralized in the water column assuming that the profile of the downward flux of POC is given by

$$POC_{flux}(z) = F_{New,POC}\exp(z/z_e), \tag{6}$$

where z is the depth and z_e is the euphotic layer thickness (100 m).

2.5. Carbonate Production and Dissolution

[14] $CaCO_3$ is produced along with particulate organic carbon assuming an average rain ratio of 0.12, the distribution of which depends on surface temperature [*Marchal et al.*, 1998]:

$$F_{Ca,DIC} = F_{NPP,DIC}\cdot Rp \tag{7}$$

$$Rp = 0.12\frac{RPM}{\overline{RPM}} \tag{8}$$

$$RPM = \frac{p_1\exp(p_2[T-T_0])}{1+p_1\exp(p_2[T-T_0])}, \tag{9}$$

where the overbar indicates here the global areal average; p_1 = 1; p_2 = 0.6; T_0 = 5°C. The produced $CaCO_3$ is instantaneously redissolved according to an exponential decay depth dissolution profile, with a characteristic depth of 2000 m.

2.6. The ^{13}C Fractionation

[15] The isotopic components DI13C and DO13C are treated as separate tracers. DI13C has source and sink terms for air-sea exchanges, carbonate production and redissolution, and organic carbon production proportional to those of DIC, according to *Mook*'s [1986] fractionation

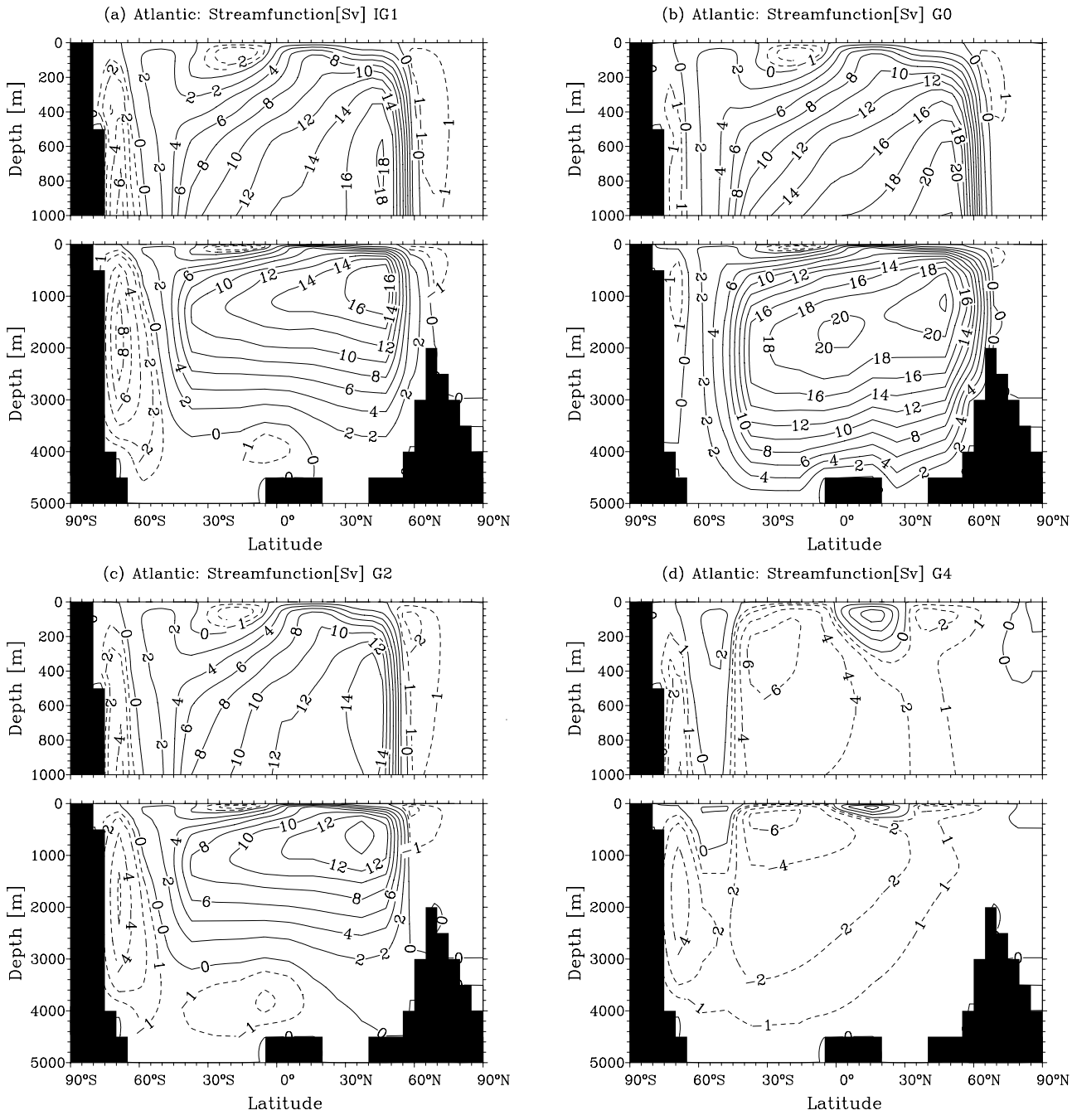

Figure 2. Atlantic stream function simulated by the model in (a) IG1 (stable with modern boundary conditions), (b) G0, (c) G2, and (d) G4' (stable (or metastable for G4') with glacial boundary conditions).

ratios for gas kinetics, air exchanges, transformation between the different forms of DIC (CO2, $HCO3^-$ and $CO3^=$), and photosynthesis. They depend on water temperature.

3. Control Experiment

[16] The control experiment consists of a 5000-year-long simulation using an atmospheric CO_2 concentration of 280 ppmv, atmospheric $\delta^{13}C = -6.5‰$ [*Wahlen*, 2002], modern ice sheets and orbital elements of 1950 A.D. Earlier simulations have shown that this model presents several stable states depending on the initial conditions [*Crucifix*, 2002]. Transitions between these states can be forced with appropriate freshwater perturbations. For consistency with earlier publications with this model, we discuss here the biogeochemical tracer distribution corresponding to the state, called IG1, where deep water formation takes place between 50° and 60°N in the Atlantic. As developed hereinafter, it presents a fairly convincing distribution of deepwater masses, but attention should be paid to its having

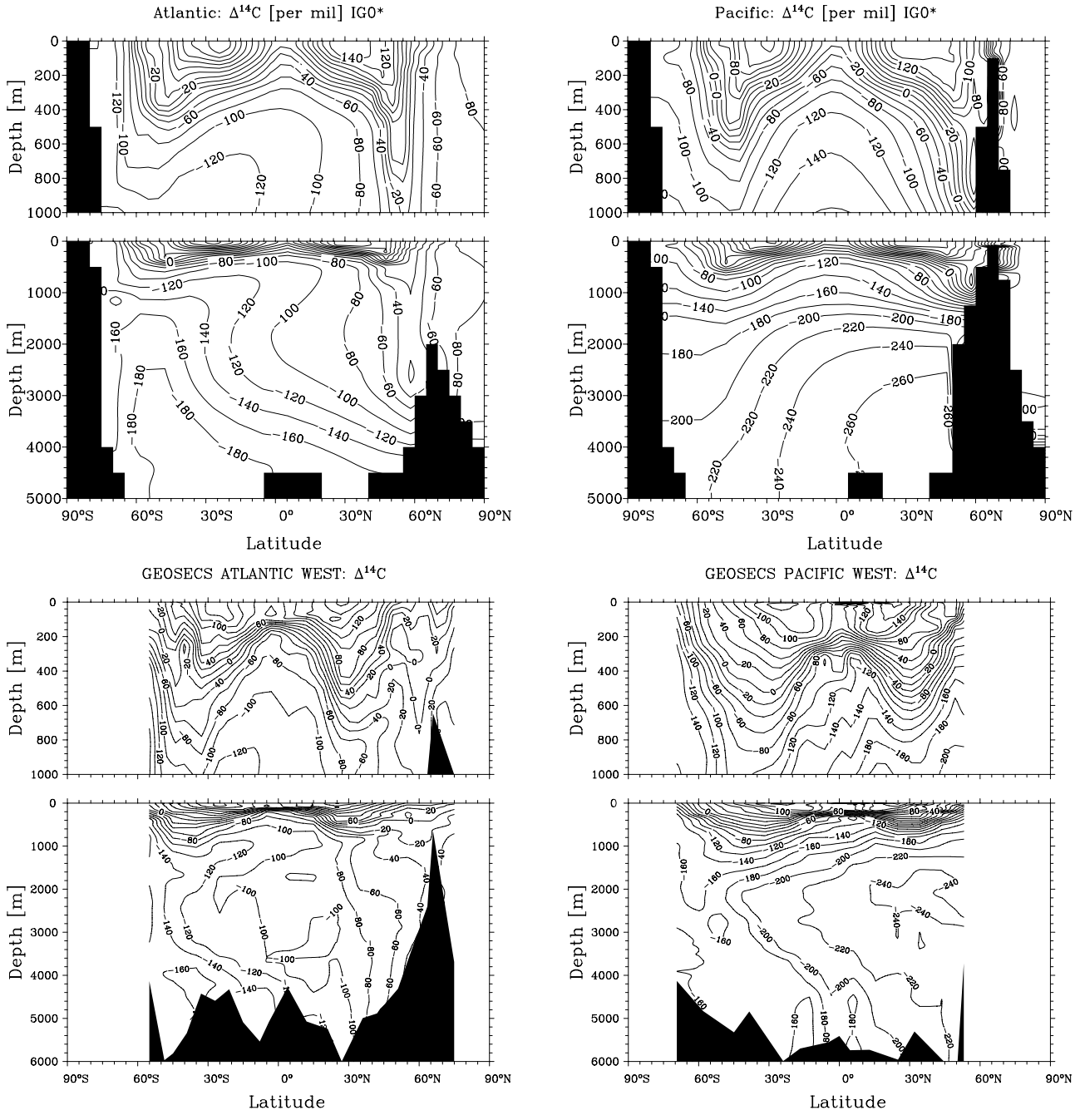

Figure 3. Distribution of radiocarbon, expressed by the $\Delta^{14}C$ in the (left) Atlantic and (right) Pacific. (top) Distribution in experiment IG1* (see text for details). (bottom) Geochemical Ocean Sections Study (GEOSECS) observations [*GEOSECS Operation Group*, 1987]. Positive $\Delta^{14}C$ are caused by anthropogenic emissions of radiocarbon during the twentieth century.

no water originating from the North Atlantic high latitudes, unlike the real world. The Atlantic meridional stream function is displayed in Figure 2a. It reaches a maximum of 18 Sv at 50°N (excluding the Ekman layer). The experiment was pursued 210 years during which the observed evolution of atmospheric radiocarbon between 1765 and 1975 was prescribed (data compilation by *Hesshaimer et al.* [1994]) in order to allow for a more direct comparison with the *GEOSECS Operation Group* [1987] observations. This state is called IG1*.

[17] Figure 3 shows the simulated zonally averaged distribution of radiocarbon (expressed as $\Delta^{14}C$) in the Atlantic and the Pacific, along with the Geochemical Ocean Sections Study (GEOSECS) data. Positive values of $\Delta^{14}C$ are related to anthropogenic emissions of radiocarbon during nuclear bomb tests. The order of magnitude of

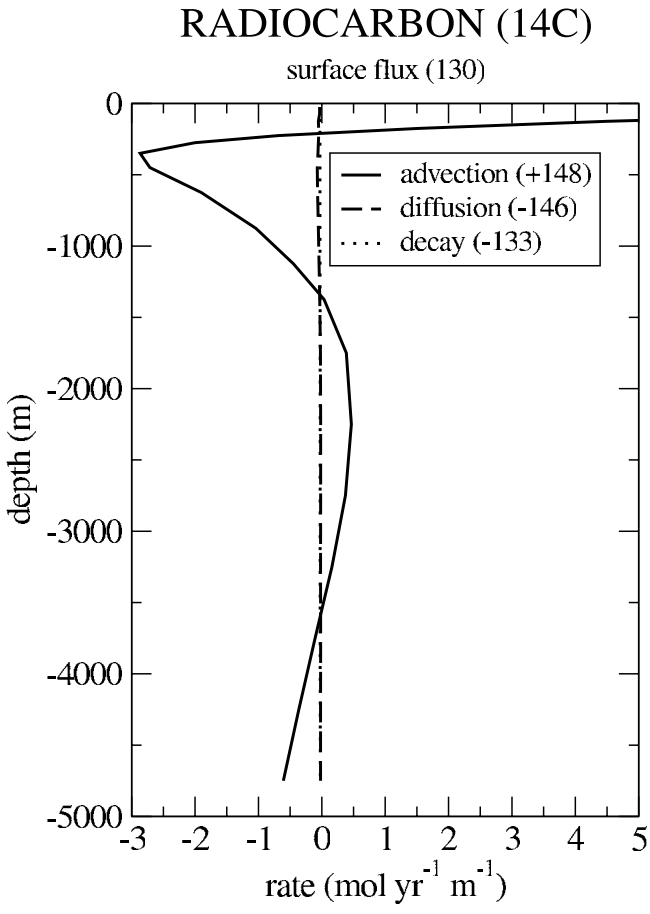

Figure 4. Depth profile of horizontal advective, diffusive, and radioactive decay contributions to the radiocarbon budget of the Southern Ocean (defined as south of 30°S). Numbers within parentheses are depth integrals (mol yr^{-1}). The net loss of radiocarbon is compensated for by a surface flux of 130 mol yr^{-1}.

abyssal water age is correct. In the Atlantic, the southward negative gradient of radiocarbon concentration resulting from the penetration of younger NADW versus older AABW is well reproduced. The Pacific deep water age is generally overestimated. Contrary to data, the minimum radiocarbon concentration is located in the bottom instead of at a depth of 2000 to 3000 m.

[18] The model has more fundamental drawbacks at intermediate depth. On the one hand, the structure of intermediate water masses is too diffusive in the Atlantic (compare the penetration of Antarctic Intermediate water with data) while, on the other hand, upwelling is too vigorous, especially in the Pacific where positive $\Delta^{14}C$ are simulated near the surface at the equator.

[19] It has been documented earlier that coarse resolution models do not correctly represent processes at the origin of intermediate water mass formation, which causes important errors in radiocarbon simulation [*Toggweiler et al.*, 1991; *Marchal et al.*, 1998]. Given the purpose of this study, it is necessary to document how the southern ocean (<30°S) radiocarbon balance is achieved despite overestimated upwelling. Figure 4 shows the contributions of advection, diffusion and radiocarbon decay to the southern ocean radiocarbon budget. The annual mean surface flux (130 mol yr^{-1}) roughly compensates for the radioactive decay. The total, depth-integrated, horizontal transport of radiocarbon into the southern ocean is close to zero. In a series of 3-D experiments with different parameterizations of the diffusive transport, *Gnanadesikan et al.* [2004] obtains greater surface fluxes (180–200 mol yr^{-1}) compensated for by a net northward transport, mainly of advective origin. By contrast, MoBidiC has a southward positive net advective component to the Southern Ocean (instead of northward). Most of this transport occurs near the surface, and it is partly compensated for at intermediate depth. Excessive upwelling also has consequences on the biogeochemical cycle, best evidenced in the Pacific distribution of apparent oxygen utilization (AOU) (i.e., the depletion in oxygen with respect to local saturation) shown on Figure 5. Compared to *Levitus and Boyer* [1994] data, the model exhibits a marked overestimation of AOU at intermediate depth around the equator. As vastly discussed in earlier works [*Najjar et al.*, 1992; *Aumont et al.*, 1999; *Oschlis*, 2000; *Brovkin et al.*, 2002], massive upwelling of inorganic nutrients produced at depth feed back productivity, which further promotes production of particulate organic material used for respiration at intermediate depth around the equator. Excessive "nutrient trapping" is known to occur in global ocean models, especially when the resolution is too coarse to correctly capture the equatorial undercurrent.

[20] Possible consequences of nutrient trapping on the biogeochemical cycle include (1) an overestimate of new production and biogenic carbonate production and (2) incorrect balance of oxygen supply to the southern ocean. As regards new production and biogenic carbonates, the zonal profiles plotted Figure 6 are fairly reassuring. Units have been chosen as to facilitate the comparison with satellite-based reconstructions of new production provided by *Gnanadesikan et al.* [2004] and inorganic carbon flux measurements provided by *Lampitt and Antia* [1997]. New production near the tropics is overestimated by around 40%, which is a reasonable performance regarding the various models discussed by *Gnanadesikan et al.* [2004]. The inorganic carbon flux at 2000 m is in good agreement with *Lampitt and Antia* [1997]. The Southern Ocean pumps 87×10^{12} mol yr^{-1} of the atmosphere. *Gnanadesikan et al.* [2004] has 86 to 194 depending on the vertical flux parameterization. However, in clear contradiction with the 3-D models, MoBidiC has a southward positive advective component overcompensated by northward eddy diffusion (Figure 7). These advective exchanges dominate above 1300 m, and result from a combination of excessive mass transport and oxygen depletion at intermediate depth.

[21] Finally, Figure 8 compares the simulated distribution of $\delta^{13}C$ in the Atlantic with the GEOSECS observations. The distribution is reasonably well captured, with a $\delta^{13}C$ of 0.8 to 1‰ for NADW, and a lower value (0.4) for AABW. The gradient of $\delta^{13}C$ at depth in the Atlantic ocean is thus

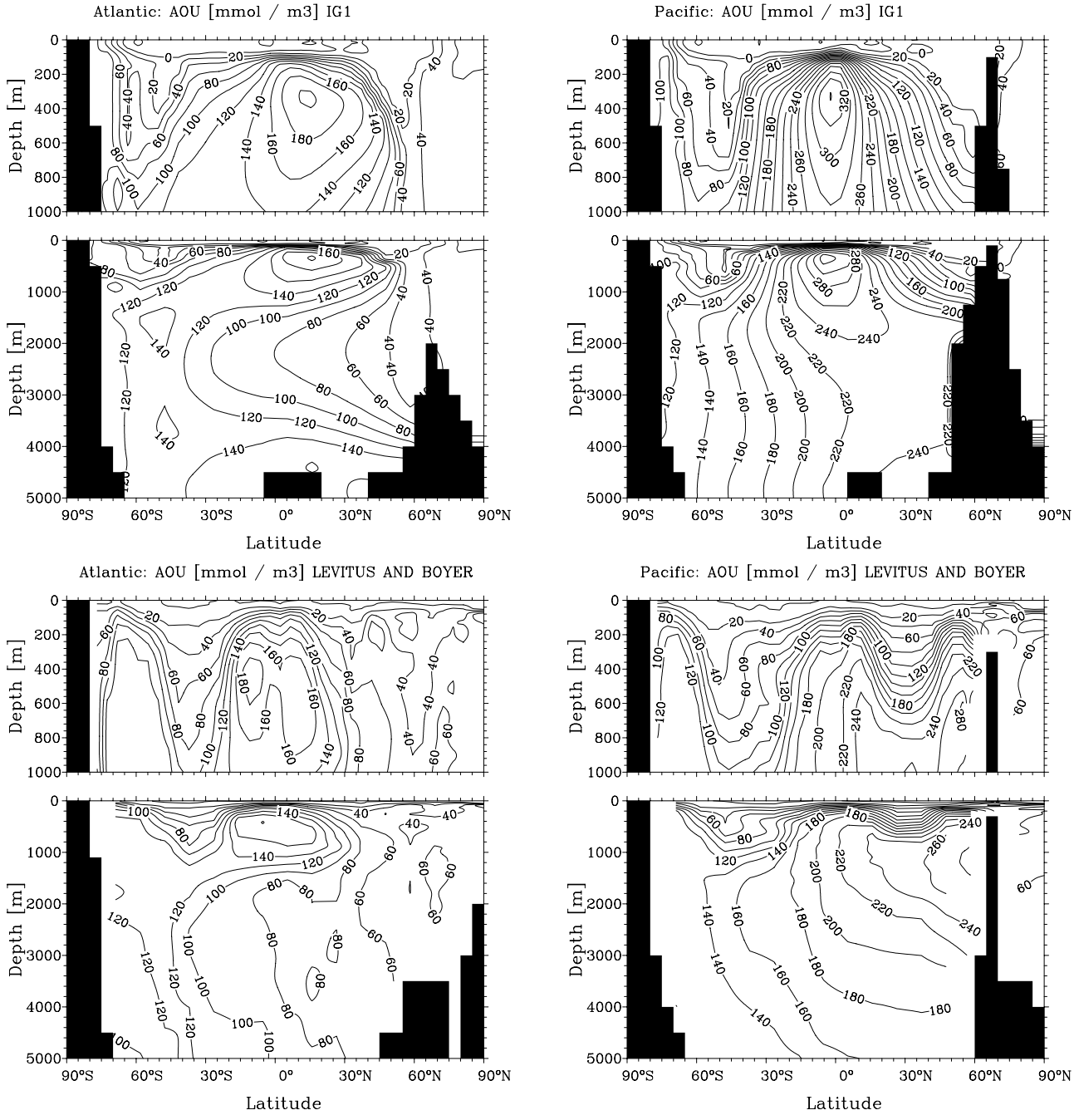

Figure 5. Zonally averaged apparent oxygen utilization (local minus saturation oxygen content) in the (left) Atlantic and (right) Pacific, simulated (top) in IG1 and (bottom) according to *Levitus and Boyer* [1994].

positive northward, as in the data. A minimum in $\delta^{13}C$ is reached at 20°N, around 300 m deep. Compared to data, this minimum is too far north and coincides with the simulated maximum of AOU.

[22] In summary, MoBidiC has a suitable representation of the structure of deepwater masses resulting from a reasonable representation of surface fluxes. However, incorrect advective exchanges taking place at and above intermediate depth produce important biases in the water properties above 1500 m. Diffusive exchanges are overall more important than in 3-D models.

4. Glacial Ocean Experiments

4.1. Model Analogues for Stadial, Interstadial, and Heinrich Climates

[23] The boundary conditions imposed in glacial-climate experiments correspond to the LGM, with CO_2 concentra-

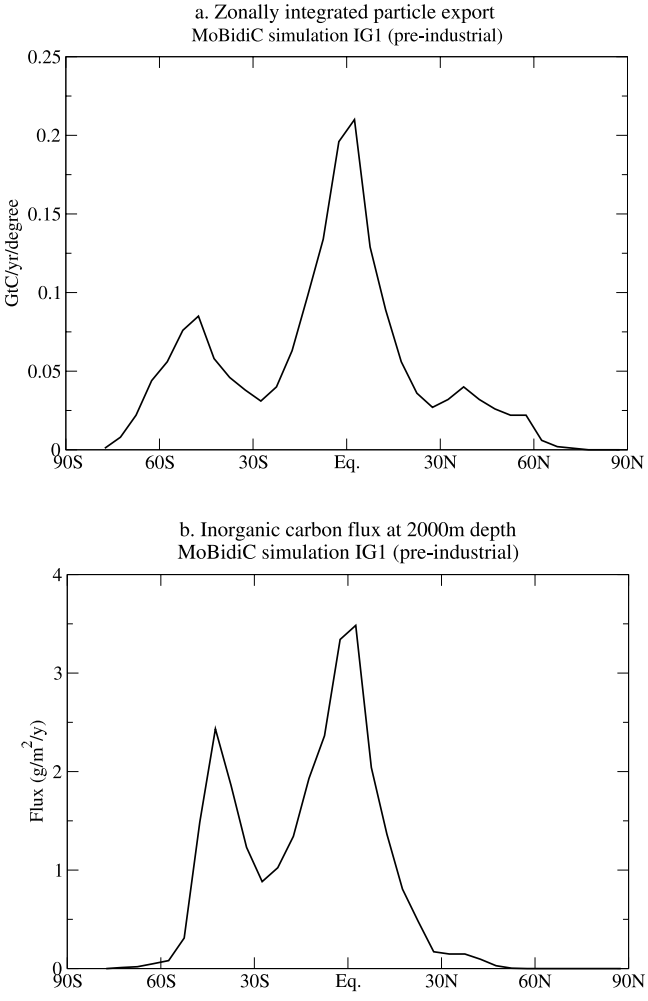

Figure 6. (a) Zonally integrated export of particulate organic carbon out of the euphotic zone simulated in MoBidiC. Units (Gt C yr^{-1} $degree^{-1}$) are chosen to compare with *Gnanadesikan et al.* [2004, Figure 7]. (b) Zonally averaged, vertical (downward) flux of $CaCO_3$, expressed in g C m^{-2} yr^{-1} to compare with *Lampitt and Antia* [1997, Figure 9].

tion of 200 ppmv, $\delta^{13}C = -6.7‰$ [*Smith et al.*, 1999; *Wahlen*, 2002], orbital parameters of 21,000 years ago [*Berger*, 1978], and northern ice sheets simulated by *Gallée et al.* [1991] for the LGM. The latter reconstruction is used because it is ideally compatible with the model structure. As for preindustrial boundary conditions, the model presents several stable solutions with last glacial maximum boundary conditions, called G0, G1 and G2. They are described by *Crucifix*, [2002]. The thermohaline circulation is broadly similar to today in all of them, but the different states differ by the position of the convection sites and the intensity of the North Atlantic overturning. In G0, convection occurs up to 65°N, and the maximum overturning is 18 Sv. As shown in Figure 2b, NADW is deeper than in the control, and AABW does not recirculate in the Atlantic. In G2, convection occurs South of 55°N (Figure 2c). The streamlines in the North Atlantic are shifted upward by about 500 m with respect to the control, and AABW recirculates more northward in the Atlantic.

[24] A complete shutoff of North Atlantic convection is not stable with glacial boundary conditions (contrary to preindustrial boundary conditions). It can however be forced with a permanent freshwater perturbation of 0.05 Sv applied to the North Atlantic surface, between 40° and 60°N. Convection recovers when the perturbation is stopped. This forced state is called G4', the corresponding stream function of which is shown in Figure 2d. Deep water forms off the Antarctic continent, and it invades the whole Atlantic volume through a reverse circulation path.

[25] The presence of several, overall active, stable states for the thermohaline circulation is a consequence, in this model, of a very efficient convective feedback [*Lenderink and Haarsma*, 1994] at northern high latitudes. This might be an artifact. However, our goal is to examine the consequences of changes in the large-scale ocean circulation on the distribution of carbon isotopes. It is therefore appropriate to analyze and compare these different equilibria.

[26] The working hypothesis formulated here is that G0, G2 and G4' are representative of the interstadial, stadial, and Heinrich states, respectively. The comparison with

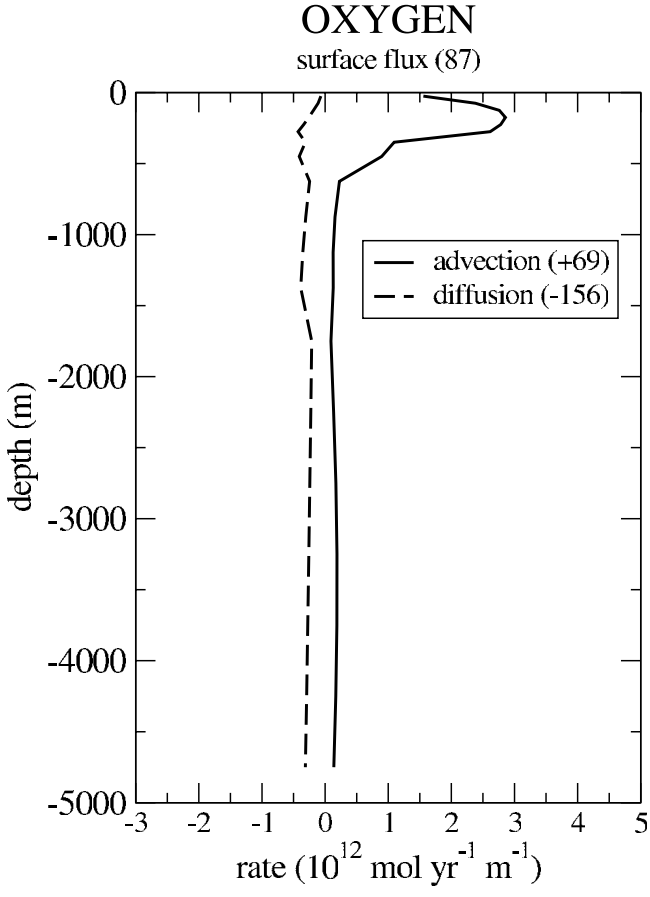

Figure 7. Same as Figure 4 but for oxygen. Units are 10^{12} mol m^{-1} yr^{-1} for the depth profile and 10^{12} mol yr^{-1} for the integral.

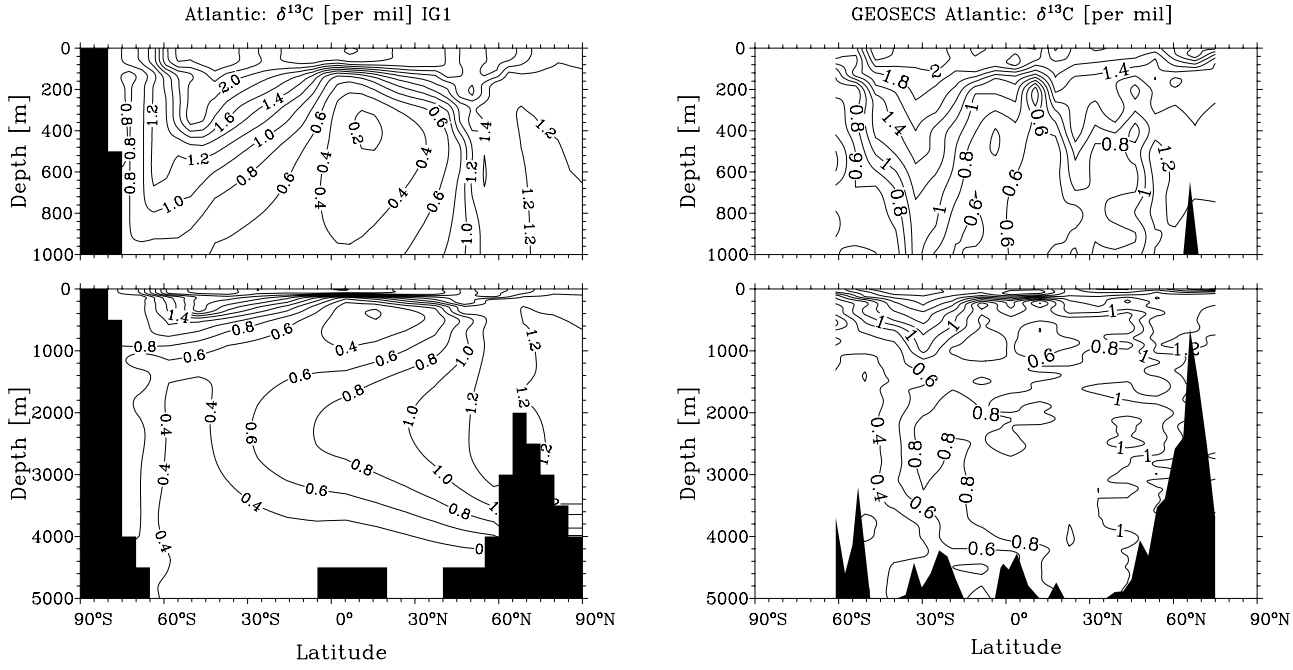

Figure 8. The $\delta^{13}C$ distribution in the Atlantic, simulated (left) in IG1 and (right) according to the observations of the western Atlantic GEOSECS transect.

data presented hereinafter assesses the relevance of this hypothesis.

4.2. Tracers Distributions in G2, G0, and G4'

4.2.1. Stadial (G2)

[27] The Atlantic radiocarbon distribution displayed on Figure 9 shows substantial differences with respect to IG1 (the differences with respect to IG1 are shown on the right-hand-side). $\Delta^{14}C$ is between -200 and -220‰ in the bottom ocean, which is about 50‰ below its preindustrial concentration. The simulated radiocarbon concentration difference between the surface and the bottom (top to bottom) is 160‰ in the midlatitude Atlantic. This is reasonable according to most recent estimates. *Keigwin* [2004] reports, for the LGM

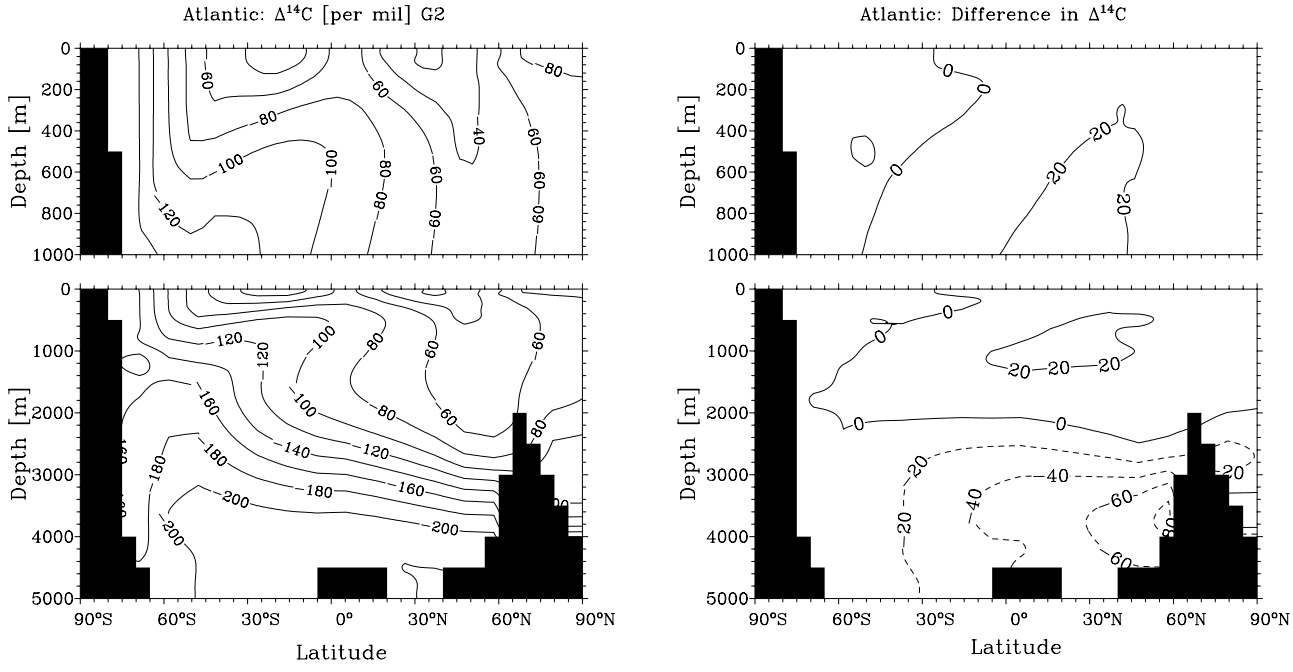

Figure 9. Distribution of $\Delta^{14}C$ in the Atlantic simulated (left) in G2 and (right) difference G2–IG1.

Table 1. Average [PO4], $\delta^{13}C$ and $\Delta^{14}C$ of NADW and AABW for the Six Experiments Presented in This Study[a]

	NADW			AABW			Bottom Atlantic				
	[PO4], mmol m^{-3}	$\delta^{13}C$, ‰	$\Delta^{14}C$, ‰	[PO4], mmol m^{-3}	$\delta^{13}C$, ‰	$\Delta^{14}C$, ‰	NADW, %	AABW, %	[PO4], mmol m^{-3}	$\delta^{13}C$, ‰	$\Delta^{14}C$, ‰
IG1	1.25	1.17	−72	1.82	0.93	−145	55	40	2.15	0.31	−173
G2	1.08	1.19	−60	2.04	0.44	−162	37	59	2.38	0.05	−210
G0	1.63	0.74	−99	1.79	0.80	−131	98	<1	2.10	0.64	−106
G4'	—	—	—	1.90	0.44	−176	<2	77	2.67	−0.36	−273
G2R	1.08	1.06	−66	2.04	0.07	−198	37	59	2.19	−0.24	−228
G2P	1.03	1.20	−60	2.03	0.29	−162	37	59	2.39	−0.11	−210

[a]NADW and AABW are defined as water where the NADW and AABW tracers exceed 0.95, respectively (see details in Appendix A). The last five columns of Table 1 give the mean tracer concentration, $\delta^{13}C$ and $\Delta^{14}C$ in the Bottom Atlantic, which is defined here as the parcel located between 15°S and 10°N and below 3750 m depth in the Atlantic Ocean.

and in the northwestern Atlantic, benthic minus planktonic ages of 600 (2590 m) to 1550 (>4500 m) years, i.e., 70 to 170‰. *Skinner and Shackleton* [2004] find a "ventilation age" of 1349 years (150‰) in the northeast Atlantic at 3146 m depth.

[28] In MoBidiC, the depletion of radiocarbon in the bottom Atlantic at the LGM is due to a more northward penetration of AABW that fills in an important fraction of the Atlantic volume. As emphasized by *Wunsch* [2003], an important reduction in $\Delta^{14}C$ may indicate a redistribution of water masses and not so much a modification in their properties. This hypothesis is verified with the help of color (passive) tracers (Table 1, see also the method explanation in Appendix A): It is seen that the simulated radiocarbon contents of NADW and AABW do not change much between IG1 and G2. However, the fraction of AABW in the bottom Atlantic is substantially larger in G2. Therefore the radiocarbon content of bottom water is decreased. The gradient of $\Delta^{14}C$ is slightly northward negative within the South Atlantic because of the ageing of Antarctic bottom water throughout its way toward the North Atlantic. This is in contrast with the modern ocean in which the $\Delta^{14}C$ gradient is southward negative. These changes in the Atlantic distribution of radiocarbon are in quantitative agreement with *Campin et al.* [1999]. Contrary to them, we do not simulate any radiocarbon concentration change in the Pacific basin larger than 20‰ (not shown). *Broecker et al.* [2004] recently highlighted that today's uncertainties of the glacial Pacific radiocarbon concentration are such that none of these results can presently be rejected.

[29] Figures 10 and 11 show the simulated distributions of nutrients and $\delta^{13}C$. These may be compared with the latest available $\delta^{13}C$ reconstruction of the LGM [*Curry and Oppo*, 2005]. The frontal structure of deep waters is in broad agreement with data, with a separation between northern and southern origin water between 2000 and 3000 m. Simulated end-member concentrations are provided in Table 1. They are roughly similar to the prein-

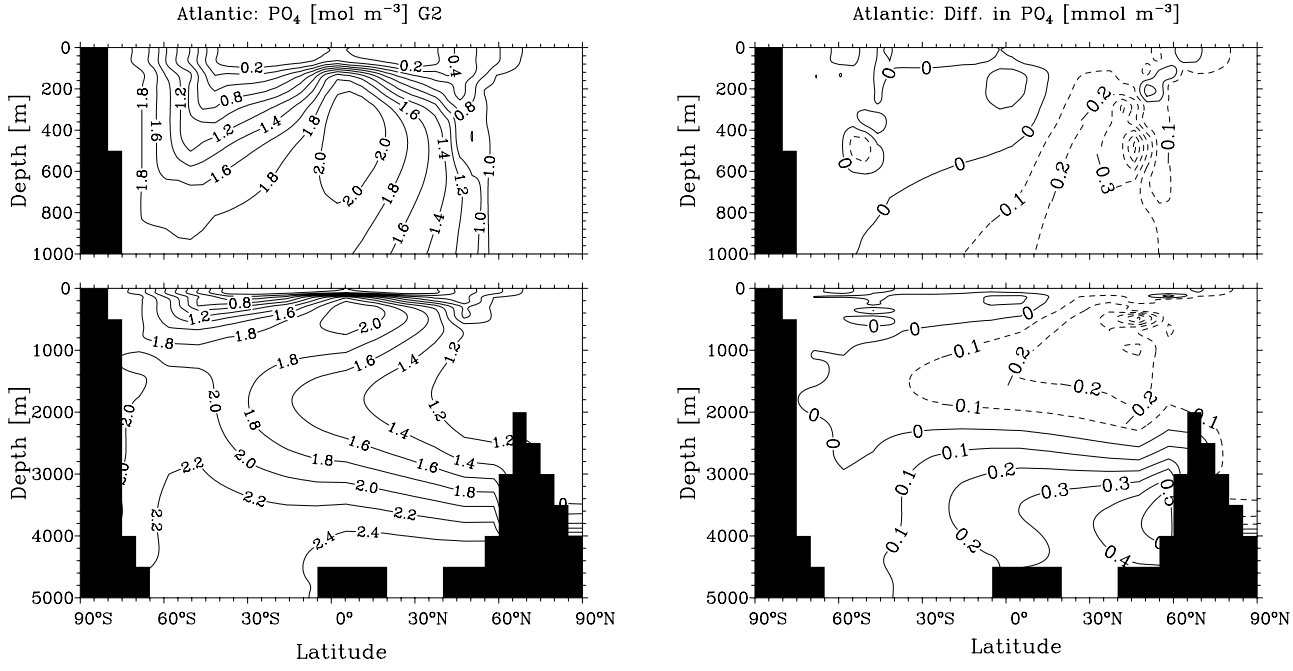

Figure 10. Distribution of phosphates [PO4] in the Atlantic simulated (left) in G2 and (right) difference G2−IG1.

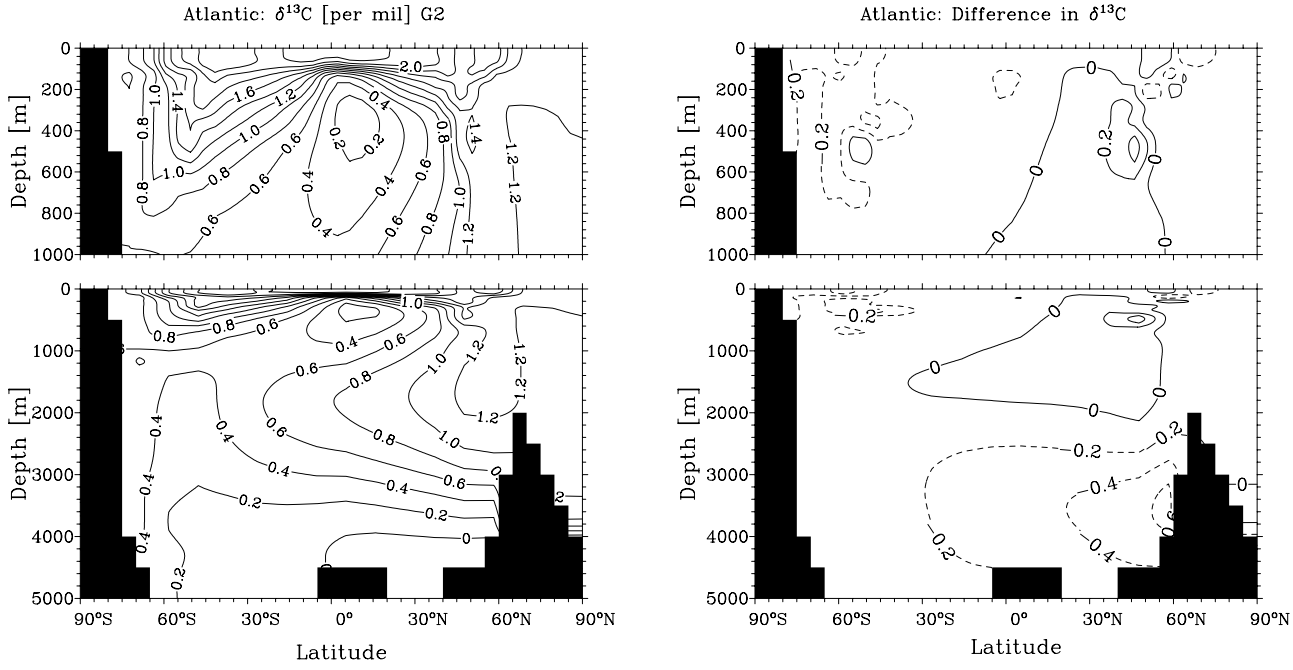

Figure 11. Distribution of $\delta^{13}C$ in the Atlantic simulated (left) in G2 and (right) difference G2−IG1.

dustrial control experiment. Maximum depletions in $\delta^{13}C$ (−280‰) and $\Delta^{14}C$ (−0.6‰) occur in the deep Pacific (not shown).

[30] On the basis of Cd/Ca ratios, *Boyle* [1992] has reported a glacial Southern Ocean nutrient concentration similar to today. By contrast, *Curry and Oppo* [2005] report important variations in end-member $\delta^{13}C$ (1.5 for North Atlantic water, and −0.9 to −0.2‰ for AABW).

[31] Much has been written about the apparent conflict between unchanged Cd/Ca and highly depleted $\delta^{13}C$ in the Southern Ocean between the LGM and today [*Boyle*, 1992; *Broecker*, 1993; *Michel et al.*, 1995]. While *Michel et al.* [1995] mainly raised arguments based on circulation, *Broecker* [1993] suggested that the anomalously low $\delta^{13}C$ concentrations in the Southern Ocean result from the dependency of air-sea fractionation on surface temperature, which

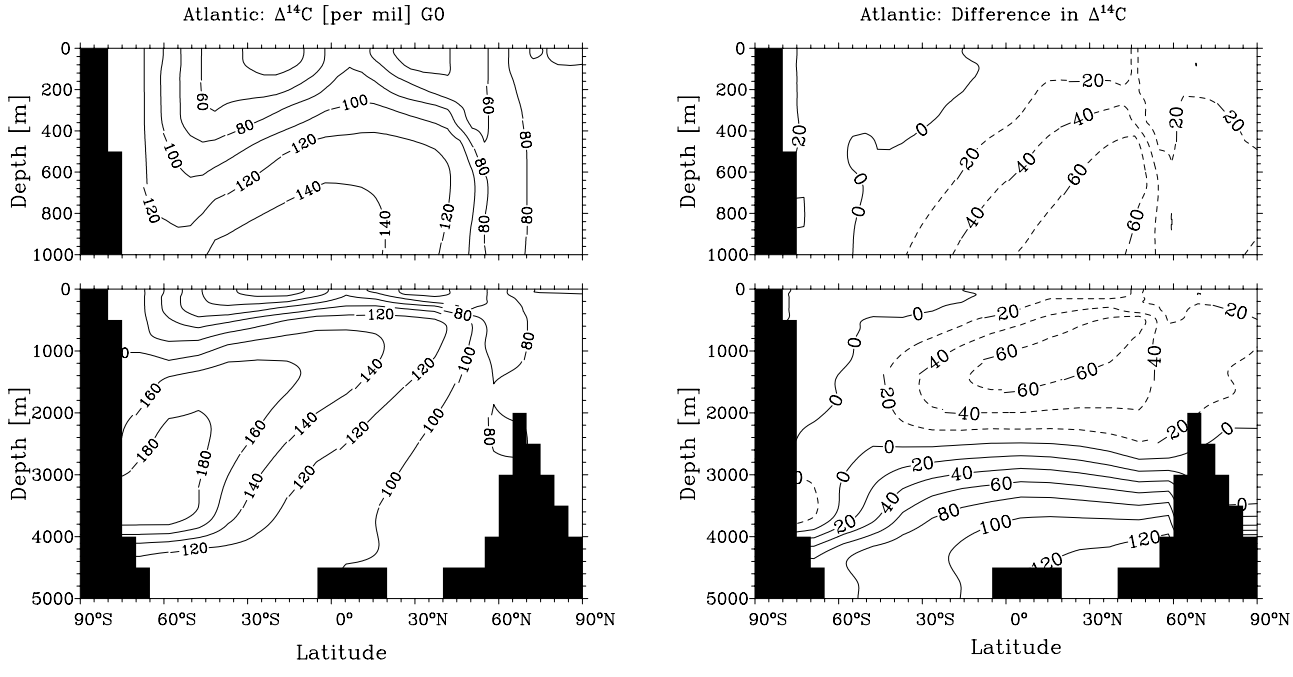

Figure 12. Distribution of $\Delta^{14}C$ in the Atlantic simulated in (left) G0 and (right) difference G0−G2.

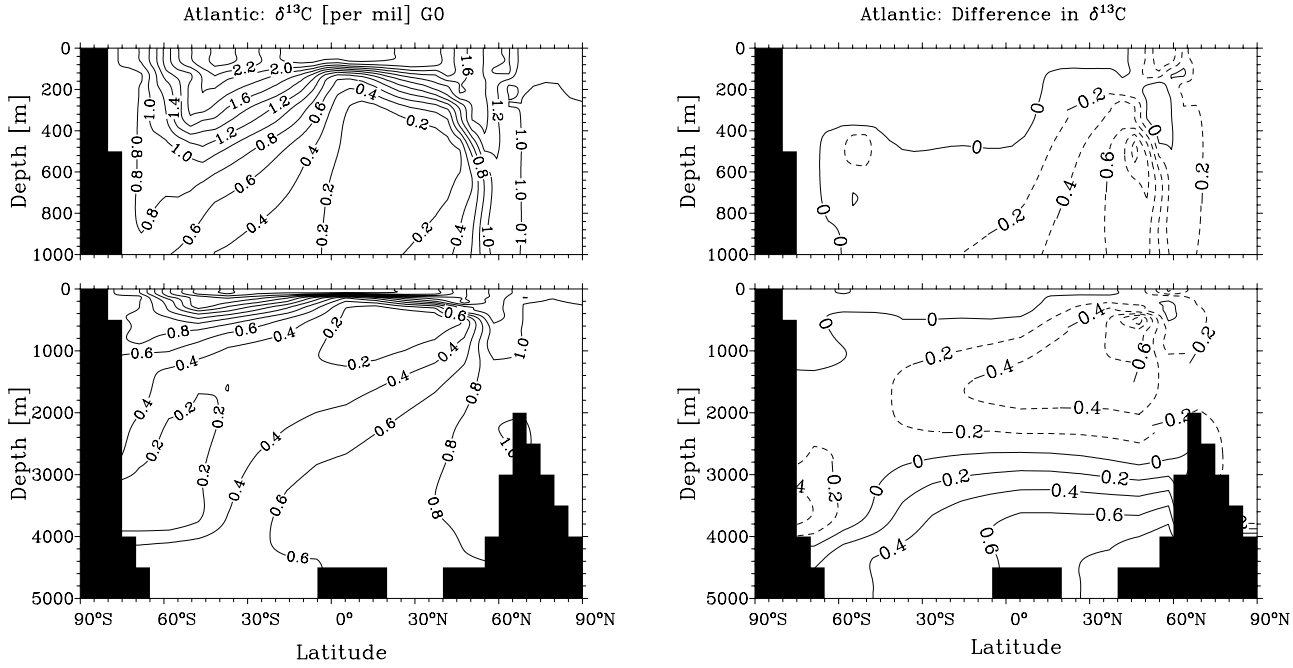

Figure 13. Distribution of $\delta^{13}C$ in the Atlantic simulated (left) in G0 and (right) difference G0−G2.

he previously documented by field measurements [*Broecker and Maier-Reimer*, 1992]. This hypothesis motivates the sensitivity experiments conducted and discussed in section 5.

4.2.2. Interstadial (G0)

[32] Figure 12 displays the distribution of $\Delta^{14}C$ in G0 and compares it to G2. The radiocarbon content of bottom water is increased by 80 to 100‰ (−640 to 800 years) as a consequence of a greater inflow of North Atlantic water. As seen in line 3 of Table 1, 98% of bottom Atlantic water is of North Atlantic origin. It is seen in Table 1 that mean radiocarbon concentration of North Atlantic Deep Water is lower in G0 (−99‰) than in G2 (−60‰), because of the higher latitude of deepwater formation in G0.

[33] There is paleoceanographic evidence for large differences in North Atlantic deep water age between interstadial and stadial phases. *Skinner and Shackleton* [2004] compared

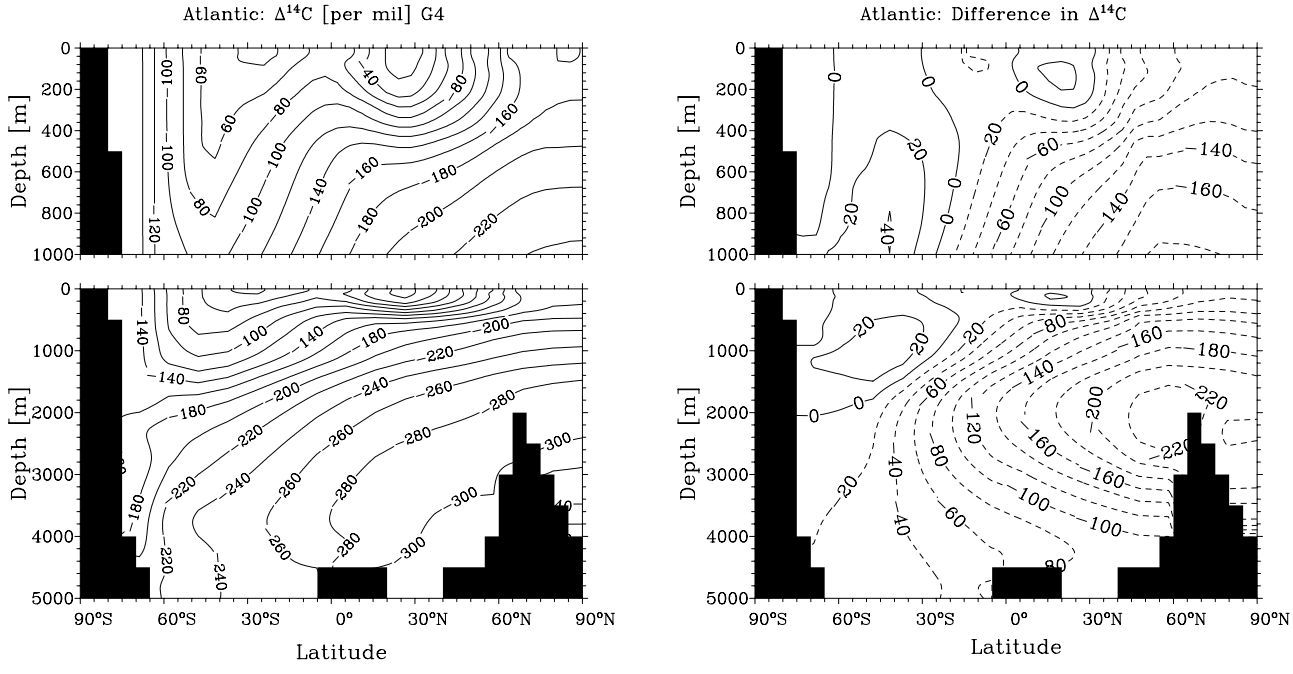

Figure 14. Distribution of $\Delta^{14}C$ in the Atlantic simulated (left) in G4' and (right) difference G4'−G2.

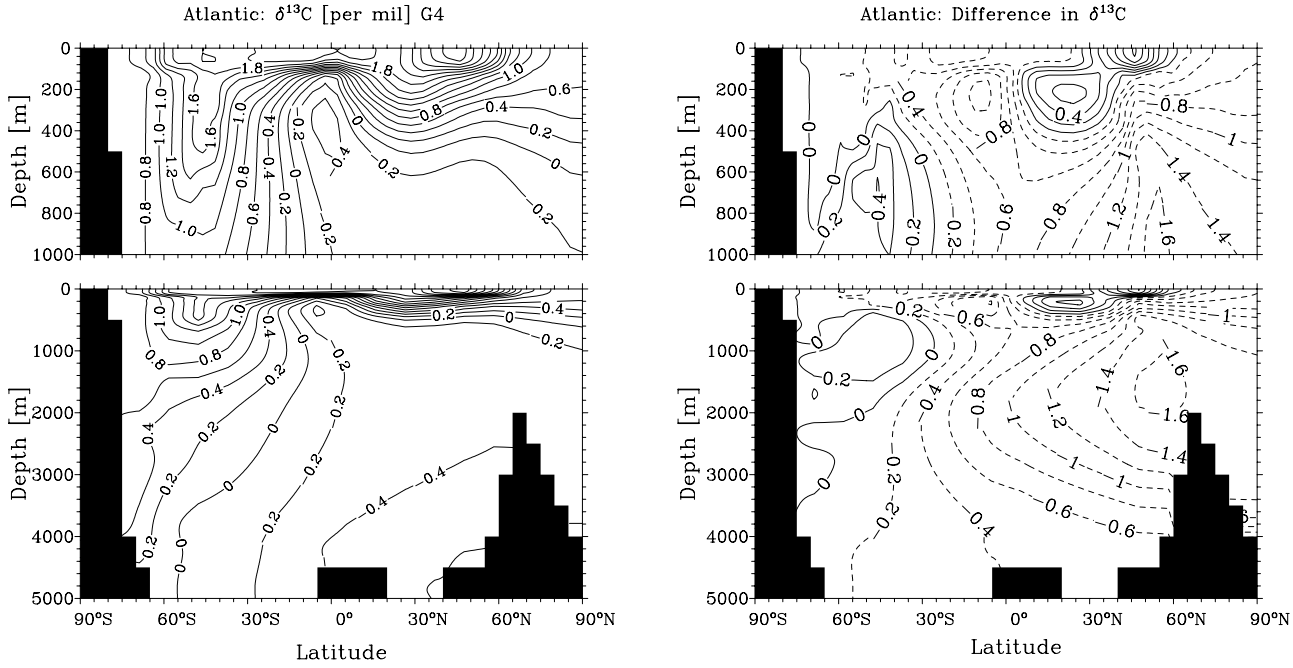

Figure 15. Distribution of $\delta^{13}C$ in the Atlantic simulated in (left) G4' and (right) difference G4'−G2.

the Bølling (interstadial) with the LGM (stadial) and found a radiocarbon age difference of about 850 years at 37°N, 3146 m depth. The increase in radiocarbon content simulated at depth is thus consistent with paleoceanographic evidence.

[34] By contrast, the simulated $\Delta^{14}C$ is reduced at intermediate depth. Reasons for these differences may easily be traced back using color tracers and transport diagnosis, but given the drawbacks characterizing intermediate water production identified with the control run, it has been preferred not to report this analysis and the corresponding comparison with data. It must also be acknowledged that except for conjectures by *Kroon et al.* [1997] about the Bølling period, there is so far little or no evidence that an overturning cell significantly stronger than today may have persisted for long periods during the last glacial period.

[35] Figure 13 shows $\delta^{13}C$ in G0, plus the difference with G2. The $\delta^{13}C$ increases with respect to G2 by 0.6‰ below 4000 m, and decreases by up to 0.6.‰ at intermediate depth at northern midlatitudes. Again, simulation of intermediate water properties has to be treated with caution. It can nevertheless be noted that *Marchitto et al.* [1998] document, in agreement with the model, anticorrelated variations between intermediate and deepwater paleonutrients in the North Atlantic during the deglaciation.

[36] The simulated $\delta^{13}C$ in the bottom Southern Ocean is not noticeably different between the stadial and interstadial, but this status quo masks a substantial reorganization of water masses. In G0, the "NADW" color tracer fills in entirely the Atlantic Ocean (Table 1, line 3) and invades the Southern Ocean. The Southern Ocean water is thus mainly coming from the North Atlantic. By contrast, G2 ("stadial") has bottom Atlantic water mainly from southern origin.

4.2.3. Heinrich (G4')

[37] No deep water forms in the in the North Atlantic in G4'. Therefore the radiocarbon distribution of the ocean is determined by the circulation of AABW, which is ageing on its way from the Antarctic to the northern latitudes before filling in the entire Atlantic ocean. Compared to the "stadial" ocean (G2), the Heinrich Atlantic Ocean has lower radiocarbon concentration both at intermediate and large depth. The minimum simulated $\Delta^{14}C$ is −300‰ (Figure 14), which is less than any water of the modern ocean. Also noteworthy is the decrease by 60 to 100‰ of surface water $\Delta^{14}C$, north of 40°N in the Atlantic. *Walbroeck et al.* [2001] estimated the surface reservoir age in the North Atlantic, north of 40°N, to be 1940 years during HE1. The simulated age of near-surface water is not so high (less than 1300 years). It was noted earlier that diffusion and upwelling are overestimated in MoBidiC. This may explain the difference between the data and the simulation. *Delaygue et al.* [2003] addressed this question by means of a large number of sensitivity experiments to wind stress and vertical eddy diffusion in a model similar to MoBidiC. As concerns deep water, *Skinner and Shackleton* [2004] give, for HE1, a ventilation age estimate of 2582 years at 37°N, 3146 m depth. This is quantitatively compatible with the simulated $\Delta^{14}C$ depletion by 290‰ at that location (equivalent radiocarbon age of 2835 years).

[38] The $\delta^{13}C$ (Figure 15) in G4' is also particularly low, down to −0.4, with a gradient negative northward, consistently with the route of AABW. Our simulation is in fairly good agreement with the reconstruction published by *Sarnthein et al.* [1994] for Heinrich event 1, but according to *Skinner and Shackleton* [2004], the simulated depletion in $\delta^{13}C$ may be overestimated. Note that *Vidal et al.* [1997] highlighted that tracer distributions of the different Heinrich events of the last glacial era are not identical.

[39] In summary, G0, G2 and G4' turn out to be reasonable analogues of the interstadial, stadial and Heinrich states

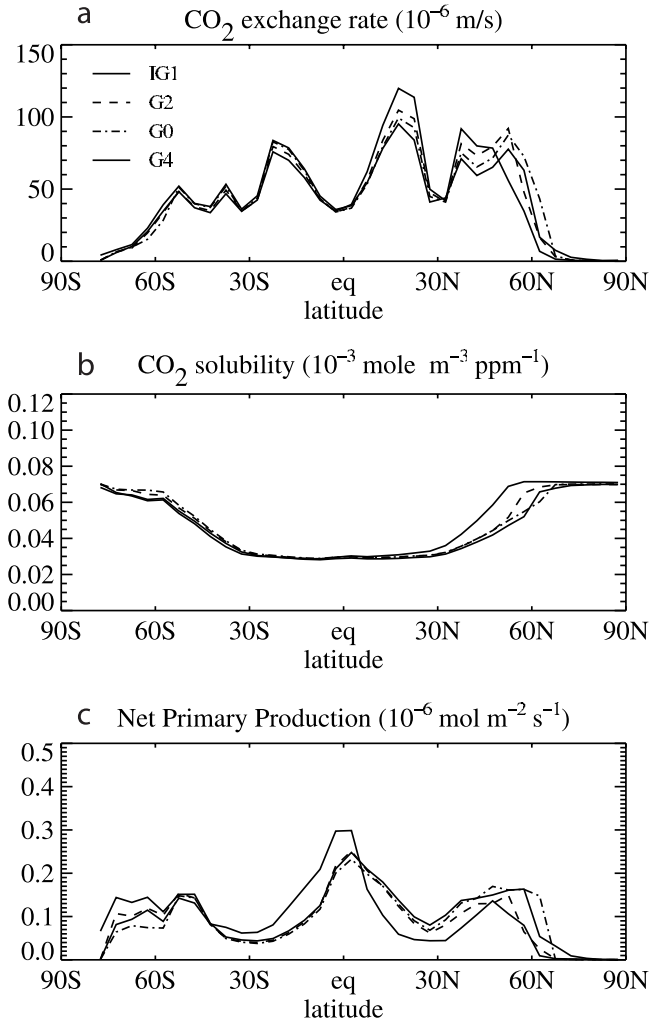

Figure 16. Horizontal distribution of annual mean (a) air sea piston velocity of CO_2 (b) CO_2 solubility at surface, and (c) new production in the Atlantic for different experiments. One mol m^{-2} s^{-1} $\simeq$ 1 g C d^{-1} m^{-2}.

of the glacial ocean in terms of carbon isotopes. However, the model does not properly reproduce the observed $\delta^{13}C$ in the glacial Southern Ocean. The Heinrich Atlantic Ocean is older than the stadial ocean at all depths. The ''interstadial'' ocean has younger deep water and older intermediate water, in terms of radiocarbon age, than the ''stadial'' ocean. The latter increase in intermediate water age contradicts some interpretations of the data [*Adkins et al.*, 1998; *Schröder-Ritzrau et al.*, 2003]. It must be kept in mind in this discussion that MoBidiC has an inadequate representation of intermediate water formation.

5. Sensitivity Experiments

[40] *Broecker* [1993] has hypothesized that some important variations in ocean $\delta^{13}C$ may be due to purely ''thermodynamical'' factors. Considering the measurements of air-sea fractionation published by *Mook* [1986], it must be realized that the spatial correlation of air-sea fractionation with sea surface temperature is primarily a consequence of the dependence of carbon dioxide solubility and gas exchange piston velocity on temperature. These quantities control the equilibrium $\delta^{13}C$ content of surface water for a given circulation pattern. The temperature dependence of the fractionation ratio during the phase change is of a secondary importance.

[41] Figure 16 compares the latitude profiles of the simulated CO_2 piston velocity, solubility and new production of organic carbon in the North Atlantic. The exchange rate, solubility and new production in the northern North Atlantic are smaller when convection is weaker (because of reduced surface temperature and nutrient concentration). In G4', the shutoff of the Atlantic overturning circulation causes an accumulation of nutrients and heat at midlatitudes. This results in an increase in new production as well as, but to a lesser extent, in piston velocity. This modification in the properties of the surface may potentially impact on the carbon isotopic composition of the ocean. This hypothesis is tested by means of a series of sensitivity experiments, where the seasonal cycles of piston velocity, solubility and bioproductivity simulated in G2 are prescribed to the ocean states G0 and G4'. This allows quantification of the corresponding contributions to the differences (G2−G0) and (G4'−G0), respectively.

[42] It is found that these contributions are small: less than 0.2‰ in $\delta^{13}C$, and less than 20‰ in $\Delta^{14}C$. This suggests that $\delta^{13}C$ and $\Delta^{14}C$ are primarily controlled by circulation changes. However, this cannot be accepted as entirely conclusive: The model may underestimate the responses of surface physical and biological processes to changes in ocean circulation.

[43] For this reason, two additional sensitivity experiments have been performed. G2R is as G2 but the piston velocity in the Southern Ocean (<50°S) is divided by 4. This experiment is inspired by the idea that a significant fraction of AABW at the LGM is formed under ice shelves and sea ice, that is, isolated from the atmosphere. As this feature is not explicitly represented in MoBidiC, the piston velocity is artificially reduced where AABW actually forms in the model. Figure 17 displays the resulting decreases in $\delta^{13}C$ and $\Delta^{14}C$. The differences are maximum near the southern ocean (−40 and −0.4‰, respectively), and are reduced by half in the Northern Hemisphere. The differences in terms of end-members are reported in Table 1 (line 5). Reducing gas exchanges induces a significant decoupling of $\delta^{13}C$ and nutrient concentration. However, the resulting $\delta^{13}C$ concentration of AABW still lies well above the −0.9‰ suggested by *Curry and Oppo* [2005].

[44] The second additional sensitivity experiment, G2P, is identical to G2 but the new production in the Southern ocean is multiplied by 4. This experiment is motivated by observations that a larger dust deposition rate at the Last Glacial Maximum may have enhanced the productivity of the Southern Ocean, which is today limited by availability of iron. Consequences of this increase on AABW are modest in MoBidiC: The $\delta^{13}C$ is reduced by 0.15‰; nutrient concentration varies very little. It is concluded that at the scale of the glacial-interglacial climatic transition, gas

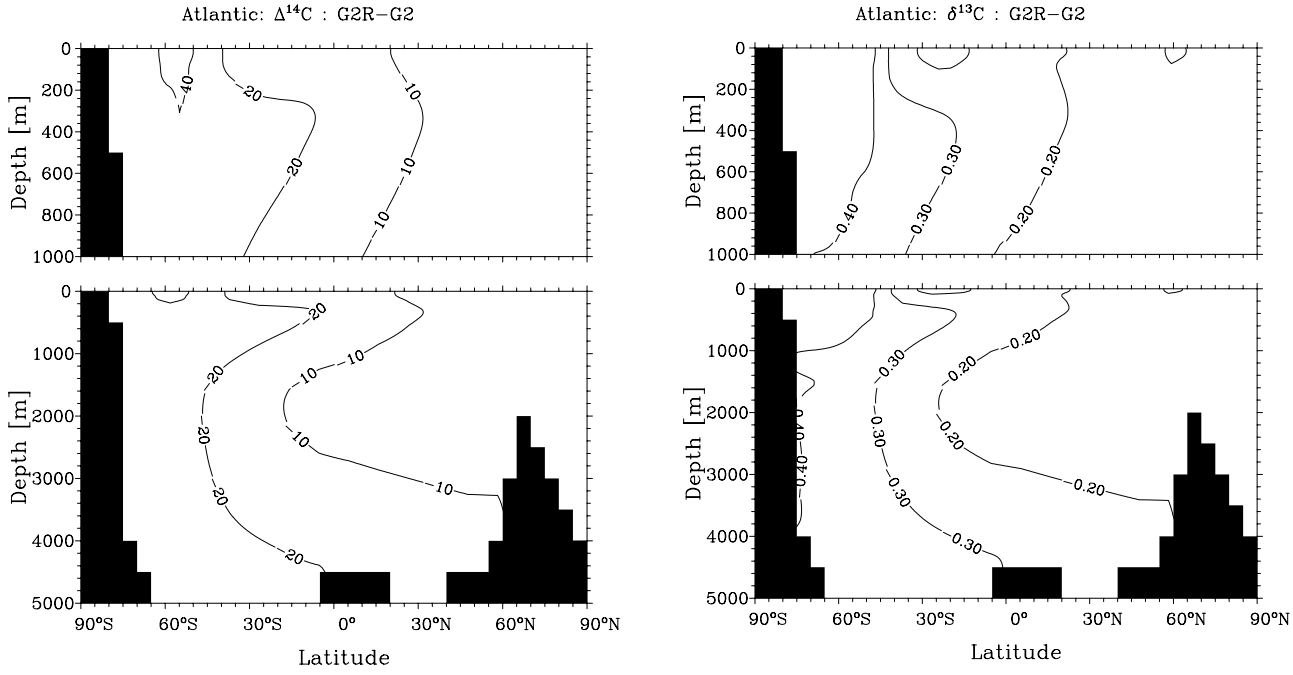

Figure 17. Difference in $\Delta^{14}C$ and $\delta^{13}C$ between experiments G2R (glacial ocean with 4 times reduced gas exchanges in Southern Ocean) and G2 (glacial ocean).

exchange has a potentially more efficient control on the isotopic composition of the ocean than bioproductivity.

6. Reconstructing Flows From ^{14}C Data

[45] It is shown above that water masses primarily determine the local $\Delta^{14}C$. We test a simple method hereinafter, requiring a small number of data points, to reconstruct the flow of North Atlantic water by combining the information provided by the color and radioactive tracer concentrations. It is assumed, to this end, that radiocarbon is conveyed by a southward advective flow of North Atlantic origin. Throughout its way to the Southern Ocean, it is mixed with water with radiocarbon concentration C_0. We use, for C_0, the radiocarbon concentration in the Southern Ocean at 60°S, 2500 m depth. Mathematical details are provided in Appendix B. Figure 18 shows the flows reconstructed for IG1, G2, G2R and G0, and compares them with the flow computed from the velocity field. It is seen that this simple scheme qualitatively captures the differences between the different equilibria (flow in G2 < IG1 < G0). The reconstructed flow is closest to the actual one around 30°N. Comparing G2 and G2R (which have the same flow) is a good test, as radiocarbon differences between G2 and G2R are of the same order of magnitude as between G2 and IG1. It is seen that the reconstructed flow for G2 and G2R differ only slightly (they would be identical if the method was perfect).

[46] Nd isotopes [*Ling et al.*, 1997] might be used as a proxy for the North Atlantic color tracer, but it may be more practical to use $\delta^{18}O$. As a test, it is attempted to infer the fraction of NADW from the salinity field (a surrogate for $\delta^{18}O$) assuming Atlantic water at 52.5°N, 50 m depth, and Southern Ocean water at 67.5°S, 50 m depth, as end-members for NADW and AABW, respectively. The flow reconstructed by this method is almost identical to that obtained with the color tracer (Figure 18b). It was also attempted to use $\delta^{13}C$ (an active tracer) to infer the proportion of NADW. In that case, the method fails (very inconsistent flows) as loss of $\delta^{13}C$ because of respiration leads to overestimate the amount of mixing. I observed that it is necessary to use averages over the vertical (1500 to 4500 m, or similar). Using grid point concentrations at a defined level (e.g., 2500) provides results exaggeratedly sensitive to the choice of end-members.

7. Conclusions

[47] This study presents results obtained with the Louvain-la-Neuve "MoBidiC" climate model including the carbon cycle. The main characteristics of the carbon cycle component are (1) a phosphorus limitation of new production, according to Michaelis-Menten kinetics; (2) a single pool of dissolved organic carbon; (3) an explicit representation of carbon isotopes ($\delta^{13}C$ and $\Delta^{14}C$); and (4) a first-order representation of the biogenic carbonate cycle with a fixed lysocline. It is found that this setup is sufficient to provide a satisfactory modern representation of ocean tracers, including oxygen, except for the presence of highly suboxic zones at intermediate depth around the equator. This problem of nutrient trapping seems common to all 2-D models discussed so far in the literature.

[48] MoBidiC has different stable states for the glacial ocean, plus one metastable state forced by a continuous freshwater discharge in the North Atlantic. The stable states differ by the position of the convection sites in the North Atlantic. By comparing model simulations with

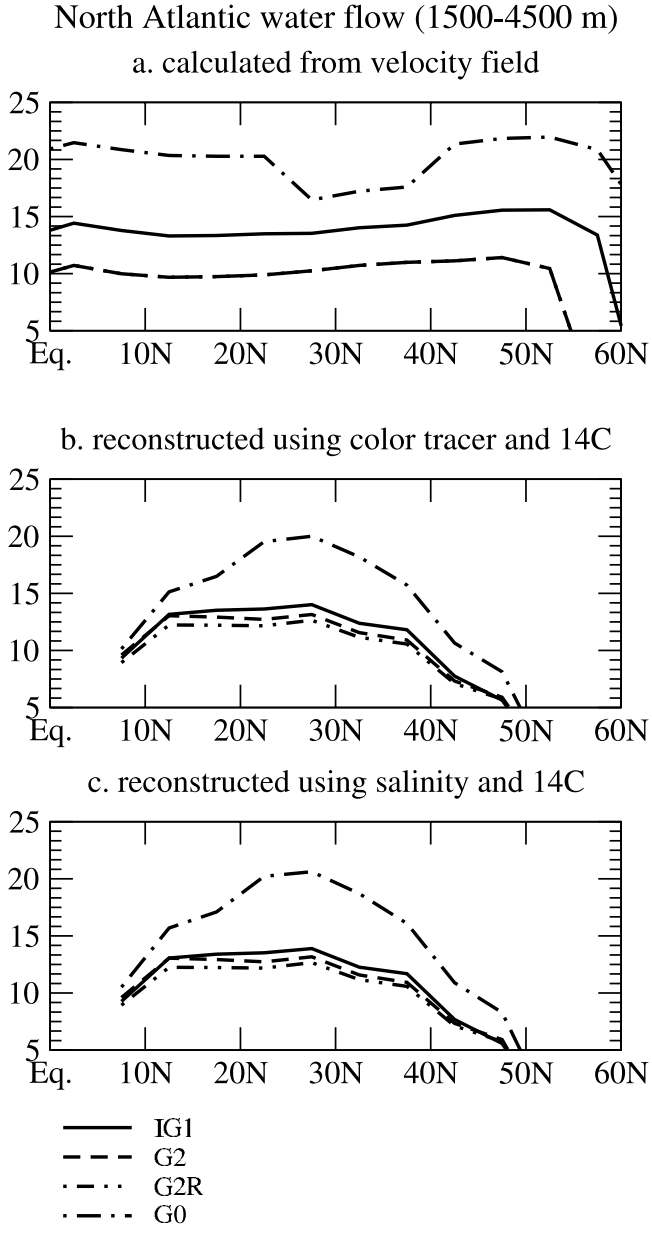

Figure 18. Water flow in the North Atlantic, between 2000 and 2500 m expressed in Sv (southward positive), in the different experiments (a) calculated from the velocity field, (b) inferred from the NADW color tracer and $\Delta^{14}C$ and (c) inferred from salinity and $\Delta^{14}C$. Reconstructions from tracers use the method described in Appendix B.

available $\Delta^{14}C$, $\delta^{13}C$ and other paleonutrient data for the deep ocean, it is suggested to use these equilibria as acceptable surrogates for the stadial, interstadial and "Heinrich" states encountered by the ocean during the last glacial era. Accepting this as a starting point, it is found that the radiocarbon age of deep water could have varied by as much as 1500 years between these different states. Comparatively, the isotopic composition of the Southern Ocean is more stable; that of the Pacific appears roughly unchanged.

[49] No entirely conclusive explanation is provided about the observed strong depletion of $\delta^{13}C$ in the Southern Ocean at the LGM. However, sensitivity experiments reveal that the gas exchange piston velocity has potentially quite an efficient control on $\delta^{13}C$: Dividing by four the gas exchange velocity between the atmosphere and the ocean off Antarctica results in a significant decoupling between nutrient concentration and $\delta^{13}C$. More explicit models of the Antarctic Bottom Water formation are needed to analyze more in-depth gas exchanges between the Southern Ocean and the atmosphere at the LGM.

[50] Information from radioactive and passive tracers can be combined to reconstruct the North Atlantic deep water flow from a simple mathematical algorithm. The scheme is simple enough to be used with actual paleoclimate data. It provides valid results for modest changes in the circulation (as between the LGM and today) but fails when the nature of the end-members determining deep north Atlantic water properties is significantly modified (e.g., Heinrich events).

[51] The present study has shown how relatively simple parameterizations for new production and isotope fractionation may provide useful information to interpret paleoclimate records. However, the 2-D model has important drawbacks in representing processes of intermediate water formation. It is therefore highly desirable to produce and document 3-D simulations with higher-resolution models.

Appendix A: Quantification of Water Masses Properties

[52] In addition to the biogeochemical tracers discussed in section 2, the ocean model includes two passive tracers with defined boundary conditions: (1) NADW, whose surface concentration equals 1 north of 40°N in the Atlantic and 0 elsewhere, and (2) AABW, whose surface concentration equals 1 south of 70°S and 0 elsewhere. By construction, the sum of NADW and AABW anywhere in the ocean is less than 1 (the remaining contributions are those from the middle_ and low_latitude Atlantic, and from the Indo_Pacific Ocean). The concentration of, say, NADW of a water parcel can be interpreted as the fraction of water in that parcel originating from north of 40°N in the Atlantic Ocean. The average [PO4], $\delta^{13}C$ and $\Delta^{14}C$ of NADW and AABW displayed in Table 1 actually represent the weighted average of these properties having more than 95% of NADW or AABW, respectively.

Appendix B: A Simple Scheme to Reconstruct Water Flow

[53] Let us consider a parcel of ocean water of volume V characterized by a passive tracer concentration a_1 and radioactive tracer concentration C_1. It is submitted to an input flow $v(1-f)$, of passive tracer of concentration a_2 and radioactive concentration C_2, and to another input flow (vf), with passive tracer concentration 0 and radioactive tracer concentration C_0. By virtue of mass conservation, input flows must be compensated for by an output flow v. Furthermore, the radioactive tracer concentration decays with time constant λ (1/8267 years for radiocarbon). Mass

conservation therefore reads (using an upwind scheme for advection):

$$(1-f)a_2 = -a_1 \quad \text{(B1)}$$

$$v[fC_0 + (1-f)(C_2) - C_1] = V\lambda C_1 \quad \text{(B2)}$$

Therefore, if passive and radioactive concentrations are known at two locations (symbolized by indices 1 and 2), the entrainment rate f and transport v between 1 and 2 can be inferred from equations (B1) and (B2) (C_0 has to be parameterized). This has been done with model outputs using the latitudinal distribution of $\delta^{13}C$, and NADW color tracers averaged between 1500 and 4500 m depth (Figure 18).

[54] **Acknowledgments.** Extensive parts of the computer code for the ocean and carbon cycle dynamics were originally written by the late Stephane Hovine (Université catholique de Louvain, Belgium) and Fortunat Joos (Bern University, Switzerland). The graphic package, based on NCAR Graphics libraries, was developed by Nicolas Gruber (UCLA, USA). Thanks are due to Jean-Claude Duplessy, Elisabeth Michel (LSCE, France), Katrin Meissner (University of Victoria, Canada), Tom Marchitto (University of Colorado, USA), and an anonymous reviewer for constructive comments and suggestions.

References

Adkins, J. F., H. Cheng, E. A. Boyle, E. R. M. Druffel, and R. L. Edwards (1998), Deep-sea coral evidence for rapid change in ventilation of the deep North Atlantic 15,400 years ago, *Science*, *280*, 280–725.

Anderson, L. A., and J. L. Sarmiento (1994), Redfield ratios of remineralization determined by nutrient data analysis, *Global Biogeochem. Cycles*, *8*, 65–80.

Aumont, O., J. C. Orr, and P. Monfray (1999), Nutrient trapping in the equatorial Pacific: The ocean circulation solution, *Global Biogeochem. Cycles*, *13*, 351–369.

Berger, A. (1978), Long-term variations of daily insolation and Quaternary climatic changes, *J. Atmos. Sci.*, *35*, 2362–2367.

Bond, G., W. Broecker, S. Johnsen, J. Mc Manus, L. Labeyrie, J. Jouzel, and G. Bonani (1993), Correlations between climate records from North Atlantic sediments and Greenland ice, *Nature*, *365*, 143–147.

Boyle, E. A. (1988), Cadmium: Chemical tracer of deepwater paleoceanography, *Paleoceanography*, *3*, 471–489.

Boyle, E. (1992), Cadmium and delta-C-13 paleochemical ocean distributions during the stage-2 glacial maximum, *Annu. Rev. Earth Planet. Sci.*, *95*, 245–287.

Boyle, E. (1995), Last-Glacial-Maximum North Atlantic Deep Water: On, off or somewhere inbetween?, *Philos. Trans. R. Soc. London, Ser. B*, *348*, 243–253.

Broecker, W. S. (1993), An oceanographic explanation for the apparent carbon isotope-cadmium discrepancy in the glacial Antarctic, *Paleoceanography*, *8*, 137–139.

Broecker, W. S., and E. Maier-Reimer (1992), Influence of air-sea exchange on the carbon isotope distribution in the sea, *Global Biogeochem. Cycles*, *6*, 315–320.

Broecker, W. S., E. Clark, I. Hajdas, and G. Bonani (2004), Glacial ventilation rates for the deep Pacific ocean, *Paleoceanography*, *19*, PA2002, doi:10.1029/2003PA000974.

Brovkin, V., J. Bendtsen, M. Claussen, C. Kubatzki, V. Petoukhov, and A. Andeev (2002), Carbon cycle, vegetation, and climate dynamics in the Holocene: Experiments with the CLIMBER-2 model, *Global Biogeochem. Cycles*, *16*(4), 1139, doi:10.1029/2001GB001662.

Campin, J. M., T. Fichefet, and J. C. Duplessy (1999), Problems with using radiocarbon to infer ocean ventilation rates for past and present climates, *Earth Planet. Sci. Lett.*, *165*, 17–24.

Crucifix, M. (2002), Palæoclimate modelling over the last glacial-interglacial cycle, Ph.D. thesis, Inst. d'Astron. et de Géophys. G. Lemaî tre, Univ. catholique de Louvain, Louvain, Belgium.

Crucifix, M., P. Tulkens, and A. Berger (2001), Modelling abrupt climatic change during the last glaciation, in *The Oceans and Rapid Climate Changes: Past, Present, and Future*, *Geophys. Monogr. Ser.*, vol. 126, edited by D. Seidov, B. J. Haupt, and M. Maslin, pp. 117–134, AGU, Washington, D. C.

Crucifix, M., M. F. Loutre, P. Tulkens, T. Fichefet, and A. Berger (2002), Climate evolution during the Holocene: A study with an Earth system model of intermediate complexity, *Clim. Dyn.*, *19*, 43–60.

Curry, W. B., and D. W. Oppo (2005), Glacial water mass geometry and the distribution of $\delta^{13}C$ of ΣCO_2 in the western Atlantic Ocean, *Paleoceanography*, *20*, PA1017, doi:10.1029/2004PA001021.

Dansgaard, W., and H. Oeschger (1989), Past environmental long-term records trom the Arctic, in *The Environmental Record in Glaciers and Ice Sheets*, edited by H. Oeschger and C. J. Langway, pp. 287–318, John Wiley, Hoboken, N. J.

Delaygue, G., T. F. Stocker, F. Joos, and G.-K. Plattner (2003), Simulation of atmospheric radiocarbon during abrupt oceanic circulation changes: Trying to reconcile models and reconstructions, *Quat. Sci. Rev.*, *22*, 1647–1658.

Dickson, A. G. (1990), Thermodynamics of the dissociation of boric acid in synthetic seawater from 273.15 to 318.15 K, *Deep Sea Res., Part A*, *37*, 755–766.

Dickson, A. G., and J. P. Riley (1976), The estimation of acid dissociation constants in seawater media from potentiometric titrations with strong base II: The dissociation of phosphoric acid, *Mar. Chem.*, *7*, 101–109.

Duplessy, J.-C., N. J. Shackelton, R. G. Fairbanks, L. Labeyrie, D. Oppo, and N. Kallel (1988), Deepwater source variations during the last climatic cycle and their impact on the global deepwater circulation, *Paleoceanography*, *3*, 343–360.

Duplessy, J.-C., M. Arnold, E. Bard, A. Juillet-Leclerc, N. Kallel, and L. Labeyrie (1989), AMS ^{14}C study of transient events and of the ventilation rate of the Pacific intermediate water during the last deglaciation, *Radiocarbon*, *31*, 493–502.

Gallée, H., J. P. van Ypersele, T. Fichefet, C. Tricot, and A. Berger (1991), Simulation of the last glacial cycle by a coupled, sectorially averaged climate-ice sheet model: 1. The climate model, *J. Geophys. Res.*, *96*, 13,139–13,161.

GEOSECS Operation Group (1987), *Geosecs—Atlantic, Pacific, and Indian Ocean Expeditions*, vol. 7, Shorebased Data and Graphics, Natl. Sci. Found., Arlington, Va.

Gnanadesikan, A., J. P. Dunne, R. M. Key, K. Matsumoto, J. Sarmiento, R. D. Slater, and P. S. Swathi (2004), Oceanic ventilation and biogeochemical cycling: Understanding the physical mechanisms that produce realistic distributions of tracers and productivity, *Global Biogeochem. Cycles*, *18*, GB4010, doi:10.1029/2003GB002097.

Goyet, C., and A. Poisson (1989), New determination of carbonic acid dissociation constants in seawater as function of temperature and salinity, *Deep Sea Res., Part A*, *36*, 1635–1654.

Grousset, F. E., L. Labeyrie, J. A. Sinko, M. Cremer, G. Bond, J. Duprat, E. Cortijo, and S. Huon (1993), Patterns of ice-rafted detritus in the glacial North Atlantic (40–55°N), *Paleoceanography*, *8*, 175–192.

Heinrich, H. (1988), Origin and consequences of cyclic ice rafting in the northeast Atlantic Ocean during the past 130,000 years, *Quat. Res.*, *29*, 142–152.

Hesshaimer, V., M. Heimann, and I. Levin (1994), Radiocarbon evidence for a smaller oceanic carbon-dioxide sink than previously believed, *Nature*, *370*, 201–203.

Hovine, S., and T. Fichefet (1994), A zonally averaged, three-basin ocean circulation model for climate studies, *Clim. Dyn.*, *10*, 313–331.

Keigwin, L. D. (2004), Radiocarbon and stable isotope constraints on Last Glacial Maximum and Younger Dryas ventilation in the western North Atlantic, *Paleoceanography*, *19*, PA4012, doi:10.1029/2004PA001029.

Kroon, D., W. E. N. Austin, M. R. Chapman, and G. M. Ganssen (1997), Deglacial surface circulation changes in the northeastern Atlantic: Temperature and salinity records off NW Scotland on a century scale, *Paleoceanography*, *12*, 755–763.

Labeyrie, L., et al. (1995), Surface and deep hydrology of the Northern Atlantic Ocean during the past 150,000 years, *Philos. Trans. R. Soc. London, Ser. B*, *348*, 255–264.

Lampitt, R. S., and A. N. Antia (1997), Particle flux in deep seas: Regional characteristics and temporal variability, *Deep Sea Res., Part I*, *44*, 1377–1403.

Lenderink, G., and R. J. Haarsma (1994), Variability and multiple equilibria of the thermohaline circulation associated with deep-water formation, *J. Phys. Oceanogr.*, *24*, 1480–1493.

Levitus, S., and T. P. Boyer (1994), *World Ocean Atlas 1994*, vol. 3, *Salinity, NOAA Atlas NESDIS*, 111 pp., NOAA, Silver Spring, Md.

Ling, H. F., K. W. Burton, R. K. O'Nions, B. S. Kamber, F. von Blanckenburg, A. J. Gibb, and J. R. Hein (1997), Evolution of Nd and Pb isotopes in central Pacific seawater from ferromanganese crusts, *Earth Planet. Sci. Lett.*, *146*, 1–12.

Maier-Reimer, E. (1993), Geochemical cycles in an ocean general circulation model: Preindustrial tracer distributions, *Global Biogeochem. Cycles*, *7*, 645–677.

Marchal, O., T. Stocker, and F. Joos (1998), A latitude-depth, circulation-biogeochemical ocean model for paleoclimate studies: Development and sensitivites, *Tellus, Ser. B*, *50*, 290–316.

Marchitto, T., Jr., W. B. Curry, and D. W. Oppo (1998), Millenial-scale changes in North Atlantic circulation since the last glaciation, *Nature*, *393*, 557–561.

Maslin, M. A., and N. J. Shackleton (1995), Surface water temperature, salinity, and density changes in the northeast Atlantic during the last 45,000 years: Heinrich events, deep water formation, and climatic rebounds, *Paleoceanography*, *10*, 527–544.

McManus, J. F., R. Francois, J. M. Gherardi, L. D. Keigwin, and S. Brown-Leger (2004), Collapse and rapid resumption of Atlantic meridional circulation linked to deglacial climate changes, *Nature*, *428*, 834–837.

Meissner, K. J., A. Schmittner, A. J. Weaver, and J. Adkins (2003), Ventilation of the North Atlantic Ocean during the Last Glacial Maximum: A comparison between simulated and observed radiocarbon ages, *Paleoceanography*, *18*(2), 1023, doi:10.1029/2002PA000762.

Michel, E., L. D. Labeyrie, J. C. Duplessy, and N. Gorfti (1995), Could deep subantarctic convection feed the world deep basins during the last glacial maximum?, *Paleoceanography*, *10*, 927–942.

Mook, W. G. (1986), ^{13}C in atmospheric CO_2, *Neth. J. Sea Res.*, *20*, 211–223.

Najjar, R. G., J. L. Sarmiento, and J. R. Toggweiler (1992), Downward transport and fate of organic matter in the ocean: Simulations with a general circulation model, *Global Biogeochem. Cycles*, *6*, 45–76.

Oschlis, A. (2000), Equatorial nutrient trapping in biogeochemical ocean models: The role of advection numerics, *Global Biogeochem. Cycles*, *14*, 655–667.

Sarnthein, M., K. Winn, S. J. A. Jung, J.-C. Duplessy, L. Labeyrie, H. Erlenkeuser, and G. Ganssen (1994), Changes in east Atlantic deepwater circulation over the last 30,000 years: Eight time slice reconstructions, *Paleoceanography*, *9*, 209–267.

Schmittner, A. (2003), Southern Ocean sea ice and radiocarbon ages of glacial bottom waters, *Earth Planet. Sci. Lett.*, *213*, 53–62.

Schröder-Ritzrau, A., A. Mangini, and M. Lomitschka (2003), Deep-sea corals evidence periodic reduced ventilation in the North Atlantic during the LGM/Holocene transition, *Earth Planet. Sci. Lett.*, *216*, 399–410.

Skinner, L. C., and N. J. Shackleton (2004), Rapid transient changes in northeast Atlantic deep water ventilation age across termination I, *Paleoceanography*, *19*, PA2005, doi:10.1029/2003PA000983.

Smith, H. J., H. Ficher, D. Mastroianni, B. Deck, and M. Wahlen (1999), Dual modes of the carbon cycle since the Last Glacial Maximum, *Nature*, *300*, 248–250.

Stocker, T. F. (1998), The effect of a succession of ocean ventilation changes on C-14, *Radiocarbon*, *40*, 359–366.

Toggweiler, J. R., K. Dixon, and W. S. Broecker (1991), The Peru upwelling and the ventilation of the south-Pacific thermocline, *J. Geophys. Res.*, *96*, 20,467–20,497.

Vidal, L., L. Labeyrie, E. Cortijo, M. Arnold, J. C. Duplessy, E. Michel, S. Becqué, and T. C. E. van Weering (1997), Evidence for changes in the North Atlantic Deep Water linked to meltwater surges during the Heinrich events, *Earth Planet. Sci. Lett.*, *146*, 13–27.

Wahlen, M. (2002), Carbon-isotopic composition of atmospheric CO_2 since the Last Glacial Maximum, http://nsidc.org/data/docs/agdc/nsidc0108_wahlen/index.html, Natl. Snow and Ice Data Cent., Boulder, Colo.

Walbroeck, C., J. C. Duplessy, E. Michel, L. Labeyrie, D. Paillard, and J. Duprat (2001), The timing of the last deglaciation in North Atlantic climate records, *Nature*, *412*, 723–727.

Wanninkhof, R. (1992), Relationship between wind speed and gas exchange over the ocean, *J. Geophys. Res.*, *97*, 7373–7382.

Weiss, R. F. (1970), The solubility for nitrogen oxigen and argon in water and seawater, *Deep Sea Res. Oceanogr. Abstr.*, *17*, 721–735.

Weiss, R. F. (1974), Carbon dioxide in water and seawater, the solubility of a nonideal gas, *Mar. Chem.*, *2*, 203–215.

Winguth, A. M. E., D. Archer, J.-C. Duplessy, E. Maier-Reimer, and U. Mikolajewicz (1999), Sensitivity of paleonutrient tracer distributions and deep-sea circulation to glacial boundary conditions, *Paleoceanography*, *14*, 304–323.

Wunsch, C. (2003), Determining paleoceanographic circulations, with emphasis on the Last Glacial Maximum, *Quat. Sci. Rev.*, *22*, 371–385.

M. Crucifix, Hadley Centre for Climate Prediction and Research, Met Office, Exeter EX1 3PB, UK. (michel.crucifix@metoffice.gov.uk)